Activity standardization of two enriched 40K solutions for the determination of decay scheme parameters and the half-life

Karsten Kossert, Yuri Amelin, Dirk Arnold, Renaud Merle, Xavier Mougeot, Michael Schmiedel, Daniel Zapata Garcia

Activity standardization of two enriched ^{40}K solutions for the determination of decay scheme parameters and the half-life

Karsten Kossert[a*], Yuri Amelin[b], Dirk Arnold[a], Renaud Merle[b,c,d], Xavier Mougeot[e], Michael Schmiedel[a], Daniel Zapata-García[a]

[a] *Physikalisch-Technische Bundesanstalt (PTB), Bundesallee 100, 38116 Braunschweig, Germany*

[b] *Research School of Earth Sciences, Australian National University, Australia*

[c] *Swedish Museum of Natural History, Sweden*

[d] *Department of Earth Sciences, Natural Resources and Sustainable Development, Uppsala University, Sweden*

[e] *Université Paris-Saclay, CEA, List, Laboratoire National Henri Becquerel (LNE-LNHB), F-91120 Palaiseau, France*

[*] *corresponding author, e-mail address: karsten.kossert@ptb.de*

Abstract

In this paper we describe experiments on two enriched ^{40}K solutions to accurately determine decay data. The first solution was measured in 2004/2005 by means of a gamma-ray spectrometer with low background and a liquid scintillation (LS) counter to apply the CIEMAT/NIST efficiency tracing method. A combination of results yields an emission probability of the 1461 keV gamma-rays of P_γ=0.1030(11) which is lower than current results of data evaluations.

The activity concentration of the second solution was also determined by means of LS counting, but here, the CIEMAT/NIST efficiency tracing method as well as the TDCR method were applied. Again, the result was combined with that of independent gamma-ray spectrometry and the gamma-ray emission probability was found to be P_γ=0.1029(9) in good agreement with the result obtained from the first solution. A combination of both experiments yields P_γ=0.1029(9). The spectra of a

TriCarb LS counter were carefully analyzed and a beta minus emission probability P_{β^-} =0.8954(14) was determined. The new results for P_γ and P_{β^-} indicate that the overall probability of the decay via EC in recent data evaluations is overestimated.

The LS counting efficiencies were computed with a stochastic model and up-to-date calculations of the beta spectrum and fractional EC probabilities were used. The final activity result of the second solution is combined with the outcome of a comprehensive isotopic analysis to determine the half-life of ^{40}K which is found to be 1.2536(27) $\cdot 10^9$ years. All above-stated uncertainties are standard uncertainties (k=1).

Key words: ^{40}K; activity standardization; liquid scintillation counting; TDCR, CIEMAT/NIST efficiency tracing; branching ratio

1. Introduction

Absolute ages of rocks, minerals and meteorites are determined using decay of long-lived radioactive isotopes and accumulation of their stable decay products. For isotopic dating, the decay constant or half-life, must be precisely and accurately known. Uncertainty of the half-life directly translates into age uncertainty. Our knowledge of half-lives of many isotopes used in geochronology lags behind the constantly improving analytical precision (Begemann et al., 2001). Uncertainties in half-lives are becoming a significant, and in some cases the largest, component in total age uncertainty.

Age determination based on radioactive decay of ^{40}K by means of the ^{40}K-^{40}Ar method (Aldrich and Nier, 1948) and the ^{40}Ar/^{39}Ar method (Merrihue and Turner, 1966) is one of the most widely used isotope chronometers in earth and planetary sciences. The ongoing progress of ^{40}K-^{40}Ar dating

is backed by numerous determinations of the half-life of ^{40}K (summarized, for example, by Begemann et al. (2001) and Renne et al. (2010)), but there is a pressing need for still more precise and accurate determinations, to allow consistent integration of the age data produced by various dating methods, and enable building a unified time scale of geological, biological, and planetary evolution.

Better methods of decay counting are the key to more reliable determination of half-lives of radionuclides significant for geochronology, in particular ^{40}K. About 20 years ago, liquid scintillation (LS) counting in combination with the CIEMAT/NIST efficiency tracing (CNET) technique proved to be a robust method to determine the activity of ^{40}K solutions and from this the total ^{40}K half-life (Grau Malonda and Grau Carles, 2002; Kossert and Günther, 2004). These experiments were performed using potassium salts with natural isotopic composition and thus with very low ^{40}K content ($n(^{40}\mathrm{K})/n(\mathrm{K}) = 0.01167\%$; see, e.g., Garner et al., 1975; Wielandt and Bizzarro 2011, Naumenko et al., 2013). As a consequence, the samples had to be prepared with rather high salt concentrations to achieve a reasonable count rate and, consequently, sample compositions differed significantly from the concentrations optimal for LS such as used in analyses of radionuclides with shorter-lived radionuclides (Broda et al., 2007). Despite the efforts to optimize/increase the K salt concentration, only relatively low counting rates could be achieved. Thus, long measurement times were required and a significant dependence on background effects remains. To determine the number of potassium atoms, Grau Malonda and Grau Carles (2002) and Kossert and Günther (2004) have chosen a stoichiometric approach which requires accurate weighing of salts with high purity. This stoichiometric approach is hindered when salts are hygroscopic. In addition, the method is based on the assumption that the natural ^{40}K abundance is perfectly known and constant. The assumption of a constant ^{40}K abundance can be questioned since variabilities of the $^{41}\mathrm{K}/^{39}\mathrm{K}$ isotopic

ratio in terrestrial materials have been documented (see, e.g., Humayun and Clayton, 1995; Wang and Jacobsen, 2016; Morgan et al., 2018), though these variabilities are small.

In this paper we describe two experiments using enriched solutions with a ^{40}K abundance of about 3% that is about 265 times higher than in natural potassium. This allowed simplified sample preparations and a reduction or even elimination of various uncertainty components.

The first experiment was carried out in 2004/2005 using an enriched solution with a nominal activity concentration of about 40 Bq/g. The solution was provided by the University of Bern and, hereafter, this solution is referred to as the "K40-Bern" solution. The experimental study with this solution comprised gamma-ray spectrometry measurements with low background and LS counting measurements using the CNET method. A combination of the results yields a new value for the emission probability of the 1461- keV gamma-rays.

The second and principal experiment was carried out using another enriched solution with an activity concentration of about 159 Bq/g (see below) that is four times that of the K40-Bern solution. For the measurements of this solution, the CNET method could be supplemented by measurements with the triple-to-double coincidence ratio (TDCR) method which increases confidence in the determined activity. In several previous works, it was shown that application of both methods is very helpful for identifying potential problems (e.g., with beta spectrum shapes) and for reducing both the model dependence and the overall final uncertainty (see, e.g., Nähle and Kossert, 2011; Kossert and Mougeot, 2015; Kossert et al., 2018; Kossert and Mougeot, 2021). This second ^{40}K solution is referred to as "K40-GSC". The potassium isotopic composition in it was measured by means of total evaporation thermal ionization mass spectrometry (TE-TIMS) and incipient emission thermal ionization mass spectrometry (IE-TIMS) as described by Amelin and Merle (2021). These measurements yielded the isotopic composition normalized to a newly prepared gravimetric reference isotopic mixtures and, hence, the half-life determination in this work does neither involve

assumptions about the ^{40}K abundance in natural potassium nor the corresponding atomic mass. In addition, potential errors due to the hygroscopic behavior of the salt have been carefully evaluated and accounted for.

2 Computation of the ^{40}K LS counting efficiencies and analysis of data for CIEMAT/NIST efficiency tracing and the TDCR method

The activity concentrations of the ^{40}K solutions studied in this work were determined by means of LS counting using the CNET method and the TDCR method (Grau Malonda, 1999; Broda et al., 2007). Both techniques are well established in radionuclide metrology and were successfully applied to accurately measure activity of various radionuclides.

In this section we describe specific aspects that are relevant for the calculation of ^{40}K LS counting efficiencies. These calculations are required for the subsequent analyses to determine the decay probabilities of various decay paths and, after this, the activity. In addition, we define a nomenclature which will be used throughout this paper.

2.1 The decay pathways of ^{40}K

Figure 1 shows the decay scheme of ^{40}K. The dominant (P_{β^-}=0.8925(17); Bé et al., 2010) decay path is a third forbidden unique beta minus transition leading to the ground state of ^{40}Ca. The second important decay path is an electron-capture (EC) decay which leads to the first excited level of ^{40}Ar and is directly followed by the prominent 1461 keV gamma transition. In this paper, this EC transition is denoted as $EC_{0,1}$; and according to Bé et al. (2010) its probability is $P_{EC_{0,1}} = 0.1055(11)$. Engelkemeir et al. (1962) observed a weak beta plus transition and determined

a ratio $P_{\beta^+} / P_{\beta^-} = 1.12(19) \cdot 10^{-5}$. Although the beta plus transition can be neglected for the LS efficiency computation, its detection plays a role in evaluating a second EC transition "$EC_{0,0}$" which directly goes to the ground state of ^{40}Ar. Bé et al. (2010) evaluated $P_{\beta^+} = 0.0000100(12)$ and $P_{EC_{0,0}} = 0.002(1)$. This evaluation is based on a theoretical estimate of the $P_{EC0,0}/P_{\beta+}$ ratio. From a more accurate EC model, Mougeot (2018) obtained slightly different decay probabilities ($P_{\beta^-} = 0.8923(13)$, $P_{EC_{0,1}} = 0.1055(11)$, $P_{EC_{0,0}} = 0.00215(27)$ and $P_{\beta^+} = 0.0000100(12)$).

The above-mentioned decay probabilities of the different pathways play an essential role when using LS counting. While the counting efficiency of the beta minus transition is usually larger than 99%, the counting efficiencies of the two EC branches are only in the order of 10%. Thus, the overall calculated counting efficiency is sensitive to the ratio of the probabilities of EC and beta minus decay (Schwarz et al., 2011).

2.2 The beta spectrum of ^{40}K

The beta minus transition is of unique 3rd forbidden nature and the shape-factor function for this type of transition is often approximated by $C(W)=p^6+7(q^4p^2+q^2p^4)+q^6$ (see, e.g., Grau Malonda, 1999). In this parameterization, the λ_k parameters that enter in the definition of the shape factor are neglected (set equal to one), although they depend on the kinetic energy of the beta particle. The influence of such an approximation has already been studied elsewhere (Mougeot, 2015). In this work, the beta spectrum was calculated with an updated version of the program BetaShape using a maximum beta energy $E_{\beta,max}$= 1310.905(60) keV from the most recent atomic mass evaluation AME2020 (Wang et al., 2021). For the calculation, a previous model (Mougeot, 2017) was improved: The screening effect is precisely taken into account by the full numerical solving of the Dirac equation for a Coulomb potential of the nucleus that includes screened potentials

(Mougeot and Bisch, 2014), allowing for a more accurate shape factor than the *C(W)* previously mentioned. While the atomic exchange correction in the previous approach took only $s_{1/2}$ orbitals into account, the new method included contributions of the $p_{1/2}$ orbitals as well as a more precise consideration of the atomic energies (Hayen et al., 2018). The radiative corrections are now those considered in the high-precision study of super-allowed beta decays (Towner and Hardy, 2008; Czarnecki et al., 2004). The computed beta spectrum is shown in Figure 2 and exhibits slightly elevated probabilities at low energies due to the exchange effect. For allowed and unique forbidden beta transitions, the BetaShape calculations were found to be very reliable when comparing with spectra measured with high precision using metallic magnetic calorimeters or when applied to modern LS measurements (see, Kossert and Mougeot, 2021, and references therein). In the case of ^{40}K, the calculations are expected to be more accurate than any experimentally determined spectrum so far. Figure 2 also shows a beta spectrum that was computed with an experimental shape-factor based on the measurements of Leutz et al. (1965) who measured parts of the beta spectrum by means of solid KI scintillation detectors. The spectrum shape is similar to the calculated one. The experimental spectrum was used when assessing a related uncertainty component.

In a previous study, the K40-Bern solution was also used to obtain information on the ^{40}K beta spectrum shape using LS counting (Grau Carles and Kossert, 2007). The corresponding method requires an energy calibration with the aid of several other beta emitters. However, since the shape of the beta spectra of the radionuclides used for calibration is not always well known, the outcome of this method cannot be regarded as very precise.

2.3 Fractional EC probabilities and other decay data

The fractional EC probabilities were calculated with the BetaShape program (Version: 2.2, May 2021) from Mougeot (2018, 2019, 2021). As input, the ground-state-to-ground-state transition energy (Q^+= 1504.40 (6) keV) was taken from the AME2020 evaluation (Wang et al., 2021) and the level energy (1460.851(6) keV) was taken from Chen (2017). The calculated fractional EC probabilities are listed in Table 1. While the BetaShape code provides EC probabilities for each subshell, the stochastic model used in this work (see next section) does not consider capture of electrons from shell L3. Hence, a simplification was made applying $P_{L2'} = P_{L2}+P_{L3}$. The probabilities for EC from other shells (M and higher) are calculated as $P_{M+} = 1-P_K- P_L$.

The internal conversion (IC) coefficients for the γ transition were calculated with the conversion coefficient calculator BrIcc (v2.3S) using the "frozen orbital" approximation (Kibédi et al., 2008). However, IC plays a minor role ($\alpha_{total}=1.028\cdot10^{-4}$) for this high-energetic gamma transition in a low *Z* nucleus. Internal pair production ($\alpha_\pi=7.3\cdot10^{-5}$) as well as a weak positron branch ($P_{\beta+}$=0.00100(12)%) were neglected in this work. When using the calculated values for internal conversion and internal pair formation, we obtain

$$P_{EC_{0,1}} = \left(1+\alpha_{total}+\alpha_\pi\right) P_\gamma = 1.00018\cdot P_\gamma . \qquad (1)$$

The K fluorescence yield ω_K=0.1199(28) was taken from Bé et al. (2010). Further atomic data were determined with methods and from sources as described by Kossert and Grau Carles (2008).

2.4 LS Efficiency computation

The LS counting efficiencies were computed by means of a stochastic model (Grau Carles, 2007; Kossert and Grau Carles, 2010) which also proved to be suitable for many isotopes including radionuclides with complex decay schemes (see, e.g., Kossert et al., 2012; 2014, 2018). The stochastic model can be used for efficiency computations that are needed to apply the CNET method

as well as to analyze TDCR data. This ensures that both methods are based on the same model and that the same decay data are used.

The ionization quenching function $Q(E)$ was calculated using the method described in a previous article (Kossert and Grau Carles, 2010), taking into account the respective composition of the used LS cocktail according to Tan and Xia (2012). The *kB* parameter was chosen to be 75 μm/MeV.

When calculating the interaction of x-rays and gamma-rays, the composition of the LS cocktails is also required. In addition, the aqueous sample fraction with its salt content (KCl) was taken into account. The computation of photon interaction by means of Monte Carlo simulations within the MICELLE code requires a definition of the dimension of the liquid volume. In the case of high-energy gamma-rays, interactions in the vial walls or the optical chamber can also cause backscattered photons, i.e., photons that enter the sensitive LS volume again. A systematic study based on various Monte Carlo codes was carried out by Cassette et al. (2006) for the 835 keV gamma rays from the ^{54}Mn EC decay. The relative increase of the photon interaction probability in the LS volume can be about 8% when the backscattering effect is taken into account. A precise quantification of this effect is difficult as it requires information about the dimension and material composition of a given LS counter. In addition, further secondary effects may play an important role: The Compton scattering process can lead to high-energy recoil electrons capable of producing Cherenkov light (Thiam et al., 2010); and bremsstrahlung may also play a role.

In the case of ^{40}K, the gamma transition is in coincidence with the transition $EC_{0,1}$ which has a probability of about 10.29% as determined in this work. The counting efficiency of the gamma-ray transition alone is about 7.2%. If we assume a relative increase of 9% due to the mentioned photon backscattering and additional secondary effects, the overall ^{40}K LS counting efficiency would increase by about 0.066%. A corresponding correction is applied to all results presented in the following. Half of this correction is adopted as a related uncertainty component. A reduction of this

uncertainty component would require detailed Monte Carlo simulations that take the complex geometry and the compositions of materials into account. Moreover, the Cherenkov effect should be considered, which may also require a consideration of optical effects. It should be noted that the backscattering effect was not taken into account by Kossert and Günther (2004) and also Grau Malonda and Grau Carles (2002) did not mention such a correction. The method used here to take into account the photon backscattering effect has already been described in a paper on ^{89}Zr (Kossert et al., 2022), where the effect plays a much larger role.

For the analysis of the TDCR measurement data, asymmetries of the PMTs were taken into account by applying a minimization procedure for the stochastic model as described by Kossert et al. (2020). Considering this effect caused relative changes well below 0.05% in all cases. This can be explained by the rather high overall counting efficiency of the ^{40}K LS samples (>91%) and the fact that the TDCR counters are equipped with matched photomultiplier tubes (PMT), i.e., with sets of PMTs that have a similar quantum efficiency. For the CNET method, a potential PMT asymmetry was considered in the uncertainty assessment as described by Kossert (2021).

3 The 2004/2005 experiment with the K40-Bern solution

An enriched (n(^{40}K)/n(K) ≈3%) aqueous ^{40}KCl solution with a nominal activity concentration of 40 Bq/g was provided by the University of Bern, Switzerland. Weighed portions of about 4 g were filled into two empty polyethylene vials that are usually used for LS counting measurements. The vials are denoted as 2004-1846 and 2004-1847 and were first measured by means of gamma-ray spectrometry in PTB´s environmental radioactivity laboratory using a coaxial high-purity Germanium (HPGe) spectrometer from the Canberra company with a relative efficiency of 50%. At PTB this spectrometer is referred to as “detector #6”. A brass holder was used to ensure a well-defined geometry with high reproducibility. This geometry was also used when measuring PTB´s

activity standard solutions with ^{60}Co, ^{88}Y and ^{137}Cs to establish an energy-dependent efficiency curve. Coincidence summing effects for ^{60}Co and ^{88}Y were taken into account (Sima et al., 2001; Arnold and Sima, 2004).

The measurement times and determined activity concentrations are summarized in Table 2 and an assessment of the different uncertainty components for the measurements of vial 2004-1846 is given in Table 3. The relative deviation of the activity concentration determined from the measurements of the two vials is about 1.1%. In both vials ^{137}Cs was detected as a radioactive impurity with an activity ratio of $A(^{137}\mathrm{Cs})/A(^{40}\mathrm{K}) = 2.4(5)\cdot 10^{-4}$.

After the gamma-ray spectrometry measurements, the vial 2004-1846 was opened and four LS sources with weighed portions of about 1 g each were prepared. To this end, 20 mL glass vials were first filled with 15 mL of Ultima Gold LLT scintillation cocktail before adding the radioactive ^{40}K solution. Small amounts of nitromethane were added to some LS samples to vary the counting efficiency. The LS sources were measured in a Wallac 1414 spectrometer and analyzed with the CNET method. It should be noted, that, at the time of this experiment, neither the TDCR method nor a TriCarb LS counter were available at PTB. A few more details on the Wallac counter will be given in the description of the principal measurements (see below). Each LS sample was measured 8 times with a total counting time of 12 h per source. A correction was applied to allow for the detected ^{137}Cs impurity. The results for the activity concentration of the individual LS samples were in very good agreement; the relative standard deviation of the activity concentration was determined to be 0.125%. Thus, any significant systematic error due to a potential inhomogeneity of the solution can be ruled out. A complete uncertainty budget for this solution is shown in Table 4.

When comparing the mean value of the activity concentration obtained from LS counting (40.57 Bq/g) with that of gamma-ray spectrometry for vial 2004-1846 (39.02 Bq/g) a significant

relative deviation of about 4% was observed. It is to be noted that a gamma-ray emission probability $P_\gamma = 0.1067(13)$ (Schötzig and Schrader, 2000) and a beta emission probability of $P_{\beta^-} = 0.8913(13)$, and consequently a probability $P_{EC_{0,0}} = 0.002$, were used for these initial analyses. Figure 3 shows the initially determined values as well as curves that represent the results as a function of the gamma-ray emission probability P_γ (Note: These curves are not straight lines). A combination of the results yields a gamma-ray emission probability $P_\gamma = 0.1030(11)$. When assessing the uncertainty, we have also accounted for the fact that the EC transition to the ground state has never been observed directly, i.e., our result for P_γ and its uncertainty are also compatible with $P_{EC_{0,0}} = 0$.

The gamma-ray emission probability determined with the K40-Bern solution deviates significantly from the initial value and is still lower than the value from the most recent evaluations.

When using the decay probabilities as determined in this paper, the activity concentration of the K40-Bern solution is eventually found to be 40.42(11) Bq/g.

4 The principal experiment with the K40-GSC solution

4.1 The K40-GSC solution

Enriched ^{40}K material manufactured by ORNL/Martin Marietta was kindly provided by the Geological Survey of Canada (GSC). An aqueous KCl master solution was prepared at ANU and a weighed aliquot (~22.68 g) in a sealed 30-mL Teflon^{TM} FEP vial was shipped to PTB for activity measurements, while other aliquots were used for the isotope analysis at ANU. The nominal activity concentration of the solution was assumed to be 150 Bq/g. This estimate is made for the purpose of planning experimental work and does not propagate into the results in any way.

4.2 LS Sample preparation

At PTB, four LS samples were prepared with a 15 mL Ultima Gold^{TM} scintillator in 20 mL low-potassium borosilicate glass vials. About 0.5 mL of distilled water and weighed portions of about 500 mg of the ^{40}K solution were added to two of the samples. Two additional samples were prepared with weighed portions of about 1000 mg of the ^{40}K solution, but no distilled water was added to these samples. A corresponding background sample was prepared with 15 mL Ultima Gold scintillator and 1 mL of distilled water.

A second sample series was prepared in a similar manner using polyethylene vials instead of glass vials. The polyethylene vials were measured with TDCR counters only, whereas the glass vials were measured in all four counters described below.

After completing first measurements, small amounts of nitromethane (CH_3NO_2) were added to two of the radioactive LS samples in glass vials to vary the counting efficiencies by means of chemical quenching. The background samples were also treated with nitromethane in order to have a representative background measurement for each quench level. The other two radioactive samples were kept constant, i.e., no nitromethane was added, in order to check sample stability. After additional long measurements, further amounts of nitromethane were added to the quenched samples. In this way, variation of the counting efficiency could be applied over a wide range despite the fact that a limited amount of solution was available. The initial period of observation comprised several months, in which parallel measurements in different counters were carried out.

The masses of all samples were determined gravimetrically using two Mettler-Toledo balances (XP26/M and XP205DR/M) traceable to the German national mass standard. Corrections for buoyancy have been applied.

4.3 Adsorption test

Although Teflon™ FEP, the material of the bottle in which the solution was supplied by ANU, is known to have very low absorption compared to most plastics (Teflon™ FEP Information Bulletin, 2017), we have performed a corresponding test to verify the absence of measurable adsorption effects. Such tests are occasionally applied in similar ways to other radionuclide studies. After sample preparation, the empty original container was filled with about 24 mL of distilled water and stored for 1 day. Two standard plastic vials that are normally used for LS counting were then filled with approximately 12 mL of the water each and measured as Cherenkov samples in a TriCarb 2800 TR LS counter. A corresponding background sample was also prepared. The net counting rates of the Cherenkov samples were found to be approximately 0.38 s^{-1}. The Cherenkov counting efficiency has been estimated to be 40% (Grau Malonda and Grau Carles, 2002), and, consequently, the total activity in the rinsing water is approximately 1.9 Bq which corresponds to about 12 mg of the original solution. Since the design of the container in which the solution was shipped prevents complete removal of liquid with a pipette, a remaining mass of this order of magnitude seems very plausible. So, there is no sign of any significant adsorption effect. The activity in the rinsing water corresponds to about 0.06% of the total activity and half of this was used as an uncertainty component in the final analysis to account for potential adsorption effects.

In other adsorption tests, we fill the original container with a liquid scintillator after rinsing and measure the container (e.g., ampoule) directly in a liquid scintillation counter. However, the size of the container used in this experiment made such a study impossible.

4.4 LS counters to apply the CNET method

The LS samples in glass vials were measured in a Wallac 1414 Guardian™ LS counter as well as in a TriCarb 2800 TR counter. The Wallac spectrometer is equipped with a plastic scintillation detector acting as a guard detector to suppress background events from external radiation. This

guard detector could, however, cause problems, since the 1461 keV gamma-rays from the ^{40}K LS samples could also lead to veto signals. Thus, the high-voltage supply of this guard detector was disconnected to avoid any conflict with the CNET methodology. Figure 4 shows a measured LS spectrum obtained with the Wallac apparatus. LS spectra of the TriCarb counter will be shown and discussed below in this paper.

The calibration curves, i.e., the counting efficiency of ^{3}H as a function of the quenching indicator (*SQP*(*E*) and *tSIE*, respectively*)*, were measured with the aid of a PTB standard solution of ^{3}H. The LS samples containing ^{3}H have almost the same sample composition and the same geometry as the ^{40}K LS samples, the only difference is that they contain no KCl.

4.5 TDCR counters

All LS samples were measured in two custom-built TDCR systems of PTB. The first system is referred to as TDCR-M27 (Nähle et al., 2010) and makes use of the MAC3 coincidence module (Bouchard and Cassette, 2000) with 40 ns coincidence resolving time. The second system is referred to as TDCR-M29 (Marganiec-Gałązka et al., 2018) and comprises an automated sample changer. The system is equipped with PTB's FPGA-based 4KAM coincidence module (Nähle et al., 2014). When using this counter, various coincidence resolving times were used (39.5 ns, 76.5 ns, 129.5 ns and 201.5 ns). Both TDCR systems are equipped with an optical chamber holding three Hamamatsu R331-05 photomultiplier tubes (PMTs) surrounding an LS sample in its center. Both systems are shielded with lead to reduce the background counting rate.

The anode signals of the PMTs are amplified by a CAEN N978 fast amplifier and discriminated by an Ortec 935 Constant-Fraction Discriminator. In both TDCR systems, the discrimination threshold was adjusted to just below the single electron peak.

Table 5 gives an overview on the maximum counting rates, background counting rates and counting efficiencies that were achieved with the K40-GSC LS samples in the 4 different counters. The table also contains corresponding data for the measurements with the K40-Bern solution and the experiment from Kossert and Günther (2004) who used potassium salts with natural isotopic composition. For these two experiments, only the Wallac 1414 LS spectrometer was used, since other counters were not yet available at PTB at that time. It should be noted that numerous modifications have been made to the Wallac device because of maintenance and repairs, and the location of the device has changed. These changes made over the years have led to an increase of the background counting rate.

The data in Table 5 show that the experimental conditions were considerably improved when using the K40-GSC solution; in particular, the ratios of maximum net counting rates to background counting rates are much higher when using this solution. The higher activity concentration is also an important prerequisite for sound TDCR measurements since the corresponding custom-built counters have higher background counting rates than the commercial counters used to apply the CNET method.

4.6 Determination of the branching ratio using LS spectra

Figure 5 shows a measured spectrum of a ^{40}K LS source recorded with the TriCarb 2800 TR apparatus after subtraction of a background spectrum. The major part in the spectrum (area “B”) mainly contains events due to the detection of beta electrons. At low channel numbers, the detection of EC decay events gives an additional contribution (area “A”). However, a precise separation of the areas requires assumptions on the shape of the beta spectrum contribution at low energies. In order to model this low-energy part, net spectra of LS sources of other pure beta emitting radionu-

clides were used. Figure 6 shows the low energy part of the measured ^{40}K spectrum with corresponding spectra of LS sources with ^{89}Sr, ^{14}C, ^{90}Sr and ^{90}Y, respectively. All experimental net spectra were normalized to give the same content in the sum of the channels 10-20. We define N_i(X) as the content in channel number *i* of the net spectrum of radionuclide X. The content in the area A of the ^{40}K spectrum is then determined by $N_{\mathrm{A}} = \sum_{i=1}^{10} N_i\left(^{40}\mathrm{K}\right) - N_i\left(\mathrm{X}\right)$, and the content in the area B is given by $N_{\mathrm{B}} = \sum_{l=1}^{4000} N_{\mathrm{i}}\left(^{40}\mathrm{K}\right) - N_{\mathrm{A}}$.

If the sample activity is *A*, the contribution in area A can be calculated by

$$N_{\mathrm{A}} = A\left[P_{\mathrm{EC}_{0,0}} \cdot \varepsilon_{\mathrm{EC}_{0,0}} + P_{\mathrm{EC}_{0,1}} \cdot \varepsilon_{\mathrm{EC}_{0,1}} (1-\varepsilon_{\gamma}) \right], \qquad (2)$$

i.e., it is taking into account that the branch $EC_{0,1}$ to the excited level does only contribute to area A if the gamma-ray is not detected. The dominant gamma interaction process is Compton scattering leading to recoil electrons with high energy. Thus, we assume that the gamma-ray detection will always lead to contributions in area B.

The contribution in area B is then given by

$$N_{\mathrm{B}} = A\left[P_{\beta} \cdot \varepsilon_{\beta} + P_{\mathrm{EC}_{0,1}} \cdot \varepsilon_{\gamma} \right] \qquad (3)$$

and the ratio is then

$$\frac{N_{\mathrm{B}}}{N_{\mathrm{A}}} = \frac{P_{\beta} \cdot \varepsilon_{\beta} + P_{\mathrm{EC}_{0,1}} \cdot \varepsilon_{\gamma}}{P_{\mathrm{EC}_{0,0}} \cdot \varepsilon_{\mathrm{EC}_{0,0}} + P_{\mathrm{EC}_{0,1}} \cdot \varepsilon_{\mathrm{EC}_{0,1}} (1-\varepsilon_{\gamma})} \qquad (4)$$

While the left-hand side of Eq. 4 is given by the experimental data derived from the spectrum analysis, the right-hand side of the equation can be calculated. The measurement of the ^{40}K LS source yields also a quench indicating parameter. This makes the application of the free parameter model possible: from a ^{3}H calibration measurement, we can assign a corresponding ^{3}H counting efficiency and consequently also the counting efficiencies ε_{β^-}, $\varepsilon_{\mathrm{EC}_{0,0}}$, $\varepsilon_{\mathrm{EC}_{0,1}}$ and ε_{γ} of the ^{40}K decay

components. As remaining variables, we have the decay probabilities P_{β^-}, $P_{\mathrm{EC}_{0,1}}$ and $P_{\mathrm{EC}_{0,0}}$. If we first assume that $P_{\mathrm{EC}_{0,0}}$ = 0.2% is constant, we can substitute $P_{\mathrm{EC}_{0,1}}$ with 1- $P_{\mathrm{EC}_{0,0}} - P_{\beta^-}$. As a consequence, the only unknown parameter in Eq. 4 is P_{β^-} which in turn can be calculated by

$$P_\beta = \frac{\frac{N_\mathrm{B}}{N_\mathrm{A}}\left[P_{\mathrm{EC}_{0,0}} \cdot \varepsilon_{\mathrm{EC}_{0,0}} + \left(1-\varepsilon_{\mathrm{EC}_{0,0}}\right)\varepsilon_{\mathrm{EC}_{0,1}}\left(1-\varepsilon_\gamma\right)\right] - \left(1-P_{\mathrm{EC}_{0,0}}\right)\varepsilon_\gamma}{\varepsilon_\beta - \varepsilon_\gamma + \frac{N_\mathrm{B}}{N_\mathrm{A}}\varepsilon_{\mathrm{EC}_{0,1}}\left(1-\varepsilon_\gamma\right)}$$

A major uncertainty component in this approach is related to the assumption on the spectrum shape of area B in the range of area A, i.e., it depends on the experimental spectra that were used. Table 6 shows the corresponding individual results of P_{β^-}. Further radionuclides were tested to model the low-energy part of the spectrum. When using ^{10}Be we obtain $P_{\beta^-} = 0.8959$ and when using ^{33}P, ^{35}S, ^{45}Ca, ^{60}Co a slightly higher value (mean: $P_{\beta^-} = 0.8993$) was obtained. Spectra of these radionuclide were, however, not used for the final analysis, since a parallel analysis to determine the EC probability of ^{36}Cl indicates that the corresponding spectra would lead to an overestimation of the low-energy part. Details on this will be described in a forthcoming article.

As a final result from this spectrum analysis, the mean value of the individual results shown in Table 6 is used: $P_{\beta^-} = 0.8954(14)$. The relative uncertainty of 0.15% was estimated taking into account four uncertainty components: i) an uncertainty assigned to the modelling of the beta spectrum shape at low energies, estimated by the relative standard deviation of the results from Table 6 (0.07%); ii) a component assigned to the uncertainties of computed LS counting efficiencies which were propagated (0.11%); iii) a statistical uncertainty assuming Poisson uncertainties of the overall counts in area A (>10^5 counts, rel. uncertainty 0.31%) and area B (>$8.2 \cdot 10^6$ counts, rel. uncertainty 0.03%) which were propagated (0.04%); and iv) an uncertainty to take into account that a slight

simplification was made (0.06%). The latter uncertainty component comes from the assumption that the probability of the EC decay to the ground state of ^{40}Ar is 0.2%. Repeating the overall analysis assuming $P_{\mathrm{EC}_{0,0}} = 0$ gives a slightly different value for P_{β^-}, lower by 0.06% than the previous result. This relative deviation was adopted as the fourth uncertainty component. It also accounts for the fact that the very weak beta plus branch was neglected in this approach.

The results in Table 6 shows clearly that the probability for beta minus decay determined with this spectrum analysis is considerably higher than in recent data evaluations but in good agreement with the results from Renne et al. (2011). The higher value for P_{β^-} is also in agreement with the lower value of the gamma-ray emission probability obtained from the measurements with the K40-Bern solution.

4.7 Determination of P_γ using the K40-GSC solution

The K40-GSC solution was also measured by means of low-level gamma-ray spectrometry – similar to the K40-Bern solution. A weighed aliquot of the solution (2.04545 g) was filled into a glass ampoule that was then flame-sealed. The ampoule type and filling height correspond to a standard geometry used at PTB. Activity standards with the radionuclides ^{60}Co and ^{88}Y in the same geometry were used for calibration purposes. The activity concentrations of these solutions were determined with very low uncertainties by means of primary activity standardization techniques as described by Kossert et al. (2018) for ^{60}Co and by Marganiec-Gałązka et al. (2017) for ^{88}Y. All ampoules were measured in two coaxial HPGe spectrometers from the Canberra company. One of them (detector #6; rel. efficiency 50%) was already used for the study of the K40-Bern solution. The nominal relative efficiency of the second detector (detector #9) is 24%. The measurements used for the final result were carried out in a well-defined geometry using a specially designed

sample holder made of plastic materials; the distance between source and end cap was 41 mm. The geometry does not correspond to a standard geometry and, consequently an additional lead shielding was required to ensure complete enclosure. The sample setup that includes ampoules, sample holder and lead shielding is shown in Figure 7.

The background was measured without any ampoule as well as with an empty glass ampoule similar to those used for the samples. Additional background studies were made with an ampoule that was filled with 2 g of distilled water. The measurements were carried out in the period from 6 January 2017 to 3 April 2017. The background measurements comprise more than 300 h in total. The overall measurement times with the calibration samples with ^{88}Y and ^{60}Co were 288 h and 187 h, respectively. The ^{40}K ampoule was measured three times with a counting time of more than 133 h per run (see, Table 7).

When establishing the efficiency curves, summing corrections were taken into account with the aid of the GESPECOR Monte Carlo software (Version 4.2; Sima et al., 2001).

Figure 8 shows a gamma-ray spectrum measured with detector #6. The pronounced peak at about 1460.8 keV is assigned to ^{40}K. Potassium-40 also contributes to the peak at 511 keV due to the beta plus decay and internal pair production. However, a sound quantification of the ^{40}K contribution is hindered, since the peak contains a significant number of background events. While further peaks were identified as well-known background peaks, a peak at about 661.7 keV indicates that the solution contains a ^{137}Cs impurity; the decision threshold and the detection limit that were calculated according to ISO 11929 (2010) are shown in Table 7.

For the initial determination of the ^{40}K activity, a gamma-ray emission probability $P_\gamma = 0.1055(11)$ from Bé et al. (2010) was used. The results from the three individual ^{40}K measurements were in good agreement and are listed in Table 7. For one measurement, the ^{137}Cs activity was slightly higher than the decision threshold but lower than the detection limit. Strictly speaking,

this means that our measurement method cannot be used to quantify such a low ^{137}Cs activity; however, as a pragmatic and conservative approach we have assumed an activity ratio $A(^{137}\mathrm{Cs})/A(^{40}\mathrm{K})=1.3(13)\cdot 10^{-4}$ for the subsequent analysis of LS counting data.

As for the K40-Bern solution the result of gamma-ray spectrometry can be combined with that of LS counting (see below) to determine the gamma-ray emission probability P_γ which was found to be $P_\gamma = 0.1029(9)$. An uncertainty budget for the activity concentration determined by means of gamma-ray spectrometry is shown in Table 8 and the overall uncertainty is slightly lower than that obtained with the K40-Bern solution. The overall uncertainty without the component $u(P_\gamma)$ as stated in Table 8 and the uncertainty from the LSC method were used to calculate the uncertainty of the gamma-ray emission probability taking a correlation into account.

4.8 Summary of decay scheme parameters

So far, we have determined the gamma-ray emission probability using the K40-Bern solution as well as using the K40-GSC solution and the overall probabilities for beta minus decay and EC from LS spectrum analyses. These data need to be combined in order to obtain decay data that are then used for the activity determination and the subsequent calculation of the ^{40}K half-life.

The two determinations of the gamma-ray emission probabilities are highly correlated since almost the same techniques and detectors were used. The weighted mean and the uncertainty obtained when using the K40-GSC solution are used as our final result, i.e., we obtained $P_\gamma = 0.1029(9)$. When applying Eq. 1, the decay probability for the branch $\mathrm{EC}_{0,1}$ is found to be $P_{\mathrm{EC}_{0,1}} = 1.00018 \cdot P_\gamma = 0.1029(9)$.

When combining the probability for beta minus decay $P_{\beta^-} = 0.8954(14)$ with $P_{EC_{0,1}} = 0.1029(9)$ we obtain $P_{EC_{0,0}} = 0.0017(17)$. These probabilities are used for the analysis to determine the activity. In this way, we ensure that we do not use these decay scheme parameters from other publications and, consequently, we avoid corresponding correlations.

When considering only our measurements, it is not possible to decide whether the EC branch to the ground state exists or not.

4.9 Activity determination of the K40-GSC solution

The LS samples prepared with the K40-GSC solution were measured in the two TDCR systems and the two commercial counters for CNET application. The minimum duration of a single measurement was 1800 s and each measurement comprises several cycles. In some cases, hundreds of repeat measurements were made to improve the statistical uncertainty and to check for potential long-term instabilities. All samples were found to be stable, and no significant trends of the determined activities could be identified. An example with results of repeat measurement of one sample carried out in the counter TDCR-M27 is shown in Figure 9.

The LS samples were prepared on 28 September 2016 and the majority of measurements was carried out until January 2017. The total counting time of the ^{40}K LS measurements to obtain the final results is almost 60 days plus additional 12 days for background measurements. The LS samples with glass vials were kept in a dark place at constant temperature (~20°C) and were measured again in April 2021. For these repeat measurements of the LS sources without a quenching agent the ^{40}K counting efficiencies were found to be slightly different than in January 2017 but the results for the activity concentration were in excellent agreement with the previous results. The slight efficiency changes can be explained by the aging of the LS samples and by changes in the counters (e.g., dirt in the optical chamber). The counting efficiencies of the Wallac counter determined in

2021 were about 0.2% lower whereas the counting efficiencies of the TriCarb counter were about 0.13% higher than before. The increase of the efficiency in the latter case can be explained by a maintenance of the counter in 2020, which included a cleaning of the optical chamber and the PMT surfaces.

The excellent agreement obtained for the activity concentration indicates a remarkable long-term stability, since trends can often be observed when carrying out long-term LS measurements. Such minor trends can often be attributed to a slight yellowing of diisopropylnaphthalene-based LS cocktails that increases over time (Kossert and Nähle, 2014, 2015). The outstanding long-term stability observed here also supports the assumption that there are no short-lived radioactive impurities. The situation is a bit different for the LS sources that were quenched with nitromethane. In this case, the repeated measurements carried out in April 2021 gave activity concentrations about 0.15% lower than results obtained from the 2016/2017 measurements. However, when inspecting the LS samples in August 2021, no yellow coloration could be seen in any of the vials. Results from the repeat measurements of quenched LS sources carried out in 2021 were not taken into account in the further analysis.

The background measurements were usually carried out in a short time before or after the measurements of the radioactive ^{40}K LS sample, so that they are considered as being representative and the overall long counting times ensure low statistical uncertainties. When considering the background, a further potential effect must be considered which is related to the sample composition, as discussed by Kossert et al. (2013) for the study of ^{176}Lu (see also discussion by Kossert et al., 2015). In that experiment, rather large amounts of a Lu salt (Z=71) were used to prepare LS samples, but the background sample did not contain a comparable non-radioactive salt. Even if such a salt is not radioactive, it could lead to an elevated background since the interaction probability of

external gamma-rays within the LS sample is increased. In the case of the ^{40}K experiments described here, a similar effect is expected to be very low since the atomic numbers of potassium (Z=19) and chlorine (Z=17) are much lower than in the case of lutetium. In addition, much lower salt concentrations were used; the K40-GSC solution contains about 36 mg of KCl per 1 g of solution. The assumption that this background effect is insignificant is supported by the fact that the experimental results of the LS samples with about 500 mg and about 1000 mg of the K40-GSC solution agree very well, with a relative deviation of only 0.025%.

When analyzing data from TDCR measurements, the coincidence counting rates were corrected for accidental coincidences by applying a simple methodology proposed by Dutsov et al. (2020).

Computed LS counting efficiency curves for TDCR and CNET are shown in Figures 10 and 11. The calculations were carried out with decay scheme parameters from this work and for a sample composition with 15 mL UG and 1 mL water plus the KCl salt.

The activity concentration determined for the individual LS samples is shown as a function of the counting efficiency in Figure 12. Corrections to allow for the ^{137}Cs impurity detected by means of gamma-ray spectrometry were applied. The unweighted mean of all CNET results from Figure 12 and its overall uncertainty is found to be (158.80±0.36) Bq/g. The unweighted mean of all results from the TDCR method in Figure 12 and its overall uncertainty is (158.82±0.34) Bq/g. The unweighted mean of both methods and the uncertainty from the TDCR method are adopted as the final result from this work, a=(158.81±0.34) Bq/g.

The uncertainty budgets of both methods are shown in Table 9. The evaluation of a few uncertainty components was explained above in this article and several other uncertainty components were determined following the guidance given by Kossert et al. (2015).

Figure 12 also indicates that the results using a given method agree well, even when different counters were used. Results are also consistent when using different vials. The TDCR measurements with PE-LS vials yield slightly higher counting efficiencies, but the activity concentration obtained from these measurements is in excellent agreement with that from glass vials.

In LS counting, the coincidence resolving time can play an important role and – in particular for low-energy emitters – significant effects can be observed (see, e.g., Dutsov et al., 2021, and references therein). In this work, a potential dependence was investigated by a variation of the resolving time between about 40 ns and about 200 ns when using TDCR-M29. The data (also included in Figure 12) are shown in Figure 13. The plot does not indicate any significant correlation between the activity concentration and the resolving time.

4.10 Preparation and isotope ratio mass spectrometry of the K40-GSC solution

A comprehensive description of solution preparation and isotopic analyses by means of thermal ionization mass spectrometry was published in a separate article (Amelin and Merle, 2021), so only a brief summary is presented here. The potassium chloride was heated to constant weight at 220°C to remove absorbed moisture, and dissolved in high purity water with trace amount of HCl. The concentrations of possible impurities were measured by quadrupole inductively coupled plasma mass spectrometry. The K concentration of solution is 481.654(25) μmole/g (k=1), and its expanded relative uncertainty of 0.0103% (k=2) includes the uncertainties of weighing and impurity subtraction. The atomic abundance of ^{40}K of 3.1247(12) % (k=1) was measured with thermal ionization mass spectrometry, with calibration against a series of mixtures of gravimetrically prepared solutions of highly enriched ^{39}K and ^{41}K using the procedures of total evaporation and incipient emission to minimize the effects of isotopic fractionation during analysis.

4.11 The half-life of ^{40}K

A combination of the above-stated final results for the K40-GSC solution can be used to calculate the total ^{40}K half-life applying

$$T_{1/2} = \frac{\ln(2)\frac{n_{K-40}}{n_K} C_K N_A}{a} = (1.2536 \pm 0.0027)10^9 \text{ a}$$

where a is the activity concentration (158.81(34) Bq/g), $\frac{n_{K-40}}{n_K}$ is the atomic abundance of ^{40}K in K (3.1247(12) %), C_K is the specific K concentration (481.654(25) µmole/(g of solution)) and N_A is the Avogadro constant.

5 Discussion

5.1 Revisiting the experiment from Kossert and Günther (2004)

The total ^{40}K half-life determined in this work is longer than PTB's previous result, which was found to be 1.248(3) $\cdot 10^9$ a (Kossert and Günther, 2004). However, it is worth noting that Kossert and Günther have used different decay scheme data and corresponding uncertainties from a data evaluation (Helmer, 1998) which was considered as a standard reference at the time of the analysis. The probability of the beta minus decay ($P_{\beta^-} = 0.8914(13)$) was much lower and, consequently, the probabilities for the EC branches were larger. Kossert and Günther (2004) also considered the uncertainties of the evaluated data as being reliable and propagated them to evaluate corresponding uncertainty components for the overall uncertainty of the half-life. In addition, the photon backscattering effect as discussed in this work was not considered.

A summary of the data from Kossert and Günther (2004) together with relevant information on the samples (from Tables 2 and 3 in Kossert and Günther, 2004) is provided in Table 10. In addition, the ^{40}K counting efficiencies and the half-life determined from the individual samples were

recalculated using our new decay data as well as the improved computation model. A correction to allow for the photon backscattering effect was also applied. We emphasize, however, that this recalculation was slightly simplified, since we have not taken into account the exact sample compositions. The recalculated half-lives are by about 0.43% longer than the original values. A weighted mean of the individual experimental results shown in Table 10 using the statistical uncertainties as weights yields $T_{1/2} = 1.2533 \cdot 10^9$ a in excellent agreement with the result from this work.

When applying a similar revision to the data from Grau Malonda and Grau Carles (2002), the recalculated half-life increases by about 0.08%. Scrutinizing their work with the CIEMAT/NIST method, we believe that their uncertainty on the activity concentration is incomplete and reflects only the standard deviation of the mean of their different measurements. We have thus added all the other uncertainty components from our work (Table 9) to better estimate the standard uncertainty (k=1), which has been revised to a value of 0.004 $\cdot 10^9$ a whereas Grau Malonda and Grau Carles (2002) state the same value as expanded uncertainty (k=2). Our reevaluated uncertainty might still be underestimated.

5.2 Re-evaluation of the half-life and the branching ratios

The Decay Data Evaluation Project (DDEP) aims at carefully evaluating decay schemes and atomic and nuclear decay data for radionuclides of importance in metrology (Kellett and Bersillon, 2017). These data are officially recommended by the International Bureau of Weights and Measures (BIPM). In the latest evaluation of ^{40}K decay (Bé at al., 2010), the partial half-lives were first evaluated separately, then used to derive the probabilities of all decay branches, which served eventually to normalize the partial half-lives and evaluate the total decay half-life from the full dataset. This approach was proposed by Holden (1990) and first considered for DDEP evaluation by Helmer (1998) with slight improvements. At that time, it was necessary to deal with the scarcity

of precise and complete measurements of ^{40}K decay. The present work motivates a revision of the evaluation strategy.

Starting from the comprehensive compilation of published measurements (Bé et al., 2010), all the values have been updated using the latest, most precise isotopic abundance from Naumenko et al. (2013). In particular, we have determined that there are 1.7972(12) $\cdot 10^{18}$ atoms of ^{40}K per gram of natural K based on an average atomic mass of natural K of 39.0983(25) determined from the atomic masses given in (Wang et al., 2021). Examining closely each article, a few values have been modified based on information provided by the authors and some uncertainties, which were clearly unrealistic, have been increased. The total half-life has been evaluated only on the basis of complete measurements of ^{40}K decay. After removing the outliers, only four measurements remain, namely those from Suttle and Libby (1955), Leutz et al. (1965), Grau Malonda and Grau Carles (2002) and the present work as given in Table 11. In addition to the update of isotopic abundance, the value from Leutz et al. (1965) has also been recalculated accounting for the adjustment of their original data as described below. The measurement from Kossert and Günther (2004) is superseded by the present work and cannot be used. The remaining dataset is consistent but small. Its weighted average has been considered together with the smallest experimental uncertainty, i.e. $T_{1/2}$ = 1.2521(27) $\cdot 10^{9}$ a.

In order to obtain the probability ratio $P_{\mathrm{EC}_{0,1}} / P_{\beta^-}$, we have determined the partial decay constants of the two main transitions from the available measurements as described in the following. A dataset of 18 updated partial decay constants has been established for the beta minus decay branch and four outliers had to be removed. The dataset is discrepant because of the value of Brinkman et al. (1965) that is too high, and because of the value of Leutz et al. (1965) that has an unrealistically small uncertainty, six times smaller than the second most precise measurement. The former has

been simply ignored: other measurements led to comparable values but with much higher uncertainties, and no reason was found to increase the uncertainty from Brinkman et al. (1965). The latter was kept but its uncertainty was increased at the minimum value that leads to a consistent dataset: we thus considered a specific beta activity of 26.26(20) counts per second and per gram of natural K, which is still the most precise value of the dataset. The weighted average led to a partial decay constant of $\lambda_\beta = 4.904(19) \cdot 10^{-10}$ a^{-1}.

For the EC branch to the first excited state of ^{40}Ar, a dataset of 16 updated partial decay constants has been established, after removal of one single outlier. The dataset is consistent and the precise value from Cesana and Terrani (1977) contributes to 92% in the weighted average. This seems justifiable to us in regards to the quality of their measurement. The result is a partial decay constant of $\lambda_{EC_{0,1}} = 5.646(16) \cdot 10^{-11}$ a^{-1}.

Assuming a complete decay scheme, the transition probabilities (branching ratios) can be deduced from the relationship $P_{EC_{0,0}} + P_{\beta^+} + P_{EC_{0,1}} + P_{\beta^-} = 1$. With the partial decay constants, one deduces $P_{EC_{0,1}} / P_{\beta^-} = \lambda_{EC_{0,1}} / \lambda_{\beta^-} = 0.1151(5)$. The ratio $P_{\beta+}/P_{\beta-}$ was deduced from the three available measurements (Tilley and Madansky, 1959; Engelkemeir et al., 1962; Leutz et al., 1965), the weighted mean with minimum experimental uncertainty giving $P_{\beta+}/P_{\beta-} = 1.15(14) \cdot 10^{-5}$. The ratio $P_{EC_{0,0}} / P_{\beta^+} = 211.8(24)$ was established from theory with the BetaShape code (Mougeot, 2018; Mougeot, 2019), which is able to accurately calculate such a third forbidden unique transition. The deduced transition probabilities are then: $P_{EC_{0,0}} = 0.218(27)\%$; $P_{\beta+} = 0.00103(13)\%$; $P_{EC_{0,1}} = 10.301(49)\%$; and $P_{\beta-} = 89.48(5)\%$. They are in excellent agreement with our measured values from the present work. Taking into account the latter in the $P_{EC0,1}/P_{\beta-}$ ratio, we re-evaluated

the transition probabilities as: $P_{EC0,0}$ = 0.218(27)%; $P_{\beta+}$ = 0.00103(13)%; $P_{EC0,1}$ = 10.298(43)%; and $P_{\beta-}$ = 89.483(45)%.

From the total half-life established above, one has the total decay constant λ_{tot} = 5.536(12) $\cdot 10^{-10}$ a^{-1}. With the transition probabilities, one can then deduce the corresponding partial decay constants λ_{β} = 4.954(11) $\cdot 10^{-10}$ a^{-1}, λ_{ε} = 5.822(13) $\cdot 10^{-11}$ a^{-1}, and $\lambda_{EC_{0,1}}$ = 5.701(27) $\cdot 10^{-11}$ a^{-1}. The decay constants λ_{β} and $\lambda_{EC_{0,1}}$ are slightly different than determined above, what can easily be explained by the use of different experiments to build the different datasets. The most important point, however, is that their ratio remains identical. From these decay constants, one can finally determine a specific beta minus activity of 28.21(6) counts per second and per gram of natural K, and a specific gamma activity of 3.247(15) counts per second and per gram of natural K.

5.3 Comparison of results with data from age comparison

Our measured half-life is in very good agreement with the revised total half-life from Renne et al. (2011), who analyzed data for the Fish Canyon standard (see also, Renne et al., 2010; Schwarz et al., 2011). Their result plays an important role in geochronology applications (see, e.g., Schaen et al., 2020), and the method depends on the ^{238}U half-life. Their result is also consistent at the level of one standard deviation with our evaluated half-life, which is mainly reduced by the value from Grau Malonda and Grau Carles (2002).

In Table 12, we summarize the total and partial decay constants determined from the experiments in this work and compare them to results from Renne et al. (2011). All results agree well within uncertainties and consequently, a previously observed discrepancy between the results from the nuclear physics and the geochronology communities seems to be resolved.

However, it is to be noted, that neither our experimentally determined half-life nor the newly evaluated half-life agrees with the range given by Naumenko-Dèzes et al. (2018) who studied geological samples using ^{87}Rb-^{87}Sr and ^{40}K-^{40}Ca systems as chronometers (see, Table 11).

Acknowledgements

We wish to thank Prof. Igor Villa et al. from the University of Bern for providing the K40-Bern solution and we are grateful to Dr. Bill Davis and Dr. Mike Villeneuve, Geological Survey of Canada, for providing enriched ^{40}K that was used to prepare the K40-GSC solution. This study was supported by Australian Research Council Discovery Grant DP140101116.

References

Aldrich L. T. and Nier A. O., 1948. Argon 40 in potassium minerals. Phys. Rev. 74, 876–877.

Amelin, Y., Merle, R., 2021. Isotopic analysis of potassium by total evaporation and incipient emission thermal ionisation mass spectrometry. Chem. Geol. 559, 119976.

Arnold, D., Sima, O., 2004. Extension of the efficiency calibration of germanium detectors using the GESPECOR software. Appl. Radiat. Isot. 61, 117-121.

Bé, M.-M., Chisté, V., Dulieu, C., Mougeot, X., Browne, E., Chechev, V., Kuzmenko, N., Kondev, F., Luca, A., Glán, M., Nichols, A.L., Arinc, A., Huang, X., 2010. Table of radionuclides (Vol. 5 – A = 22 to 244). Monographie BIPM-5 Vol. 5, Bureau International des Poids et Mesures, Sèvres, ISBN-13 978-92-822-2234-8.

Begemann F., Ludwig K.R., Lugmair G.W., Min K., Nyquist L.E.., Patchett P.J., Renne P.R., Shih C.-Y., Villa I.M. and Walker R.J., 2001. Call for an improved set of decay constants for geochronological use. Geochimica et Cosmochimica Acta 65, 111–121.

Bouchard, J., Cassette, Ph., 2000. MAC3: an electronic module for the processing of pulses delivered by a three photomultiplier liquid scintillation counting system. Appl. Radiat. Isot. 52, 669-672.

Brinkman, G. A., Aten, A. H. W. Jr, Veenboer, J. Th., 1965. Natural radioactivity of K-40, Rb-87 and Lu-176. Physica 31, 1305-1319.

Broda, R., Cassette, Ph., Kossert, K., 2007. Radionuclide Metrology using Liquid Scintillation Counting. Metrologia 44, S36-S52.

Cassette, P., Ahn, G.H., Alzitzoglou, T., Aubineau-Lanièce, I., Bochud, F., Garcia Torano, E., Grau Carles, A., Grau Malonda, A., Kossert, K., Lee, K.B., Laedermann, J.P., Simpson, B.R.S., van Wyngaardt, W., Zimmerman, B., 2006. Comparison of calculated spectra for the interaction of photons in a liquid scintillator. Example of ^{54}Mn 835 keV emission. Appl. Radiat. Isot. 64, 1471-1480.

Cesana, A., Terrani, M., 1977. Gamma-ray activity determination in large volume samples with a Ge-Li detector. Anal. Chem. 49 (8) 1156-1159.

Chen, J., 2017. Nuclear Data Sheets for A=40, Nucl. Data Sheets 140, 1–376.q+

Czarnecki, A., Marciano, W.J., Sirlin, A., 2004. Precision measurements and CKM unitarity. Phys. Rev. D 70, 093006.

Dutsov, Ch., Cassette, Ph., Sabot, B., Mitev, K., 2020. Evaluation of the accidental coincidence counting rates in TDCR counting. Nucl. Instrum. Methods A 977, 164292.

Dutsov, Ch., Cassette, Ph., Mitev, K., Sabot, B., 2021. In quest of the optimal coincidence resolving time in TDCR LSC. Nucl. Instrum. Methods A 987, 164846.

Engelkemeir, D. W., Flynn, K. F., Glendenin L. E., 1962. Positron emission in the decay of ^{40}K. Phys. Rev. 126, 1818-1822.

Grau Carles, A., 2007. MICELLE, the micelle size effect on the LS counting efficiency. Comput. Phys. Commun. 176, 305-317.

Grau Carles, A., Kossert, K., 2007. Measurement of the shape-factor functions of the long-lived radionuclides ^{87}Rb, ^{40}K and ^{10}Be. Nucl. Instrum. Meth. A 572, 760-767.

Grau Malonda, A., 1999. Free parameter models in liquid scintillation counting. Colección Documentos CIEMAT. CIEMAT, ISBN 84-7834-350-4.

Grau Malonda, A., Grau Carles, 2002. Half-life determination of ^{40}K by LSC. Appl. Radiat. Isot. 56, 153-156.

Hayen, L., Severijns, N., Bodek, K., Rozpedzik, D., Mougeot, X., 2018. High precision analytical description of the allowed β spectrum shape. Rev. Mod. Phys. 90 (1), 015008.

Helmer, R.G., 1998. Table de Radionucléides.

Holden, N. E., 1990. IUPAC: Total half-lives for selected nuclides. Pure and Appl. Chem. 62 (5) 941-958.

Humayun, M., Clayton, R.N., 1995. Precise determination of the isotopic composition of potassium: Application to terrestrial rocks and lunar soils. Geochim. Cosmochim. Acta 59, 2115–2130.

ISO 11929, 2010. Determination of the Characteristic Limits (Decision Threshold, Detection Limit and Limits of the Confidence Interval) for Measurements of Ionizing Radiation Fundamentals and Application. International Standards Organisation, Geneva, Switzerland.

Kellett, M. A. and Bersillon, O., 2017. The Decay Data Evaluation Project (DDEP) and the JEFF-3.3 radioactive decay data library: Combining international collaborative efforts on evaluated decay data. EPJ Web Conf. 146, 02009.

Kibédi, T., Burrows, T.W., Trzhaskovskaya, M.B., Davidson, P.M., Nestor, C.W. (Jr.), 2008. Evaluation of theoretical conversion coefficients using BrIcc. Nucl. Instrum. Meth. A 589, 202-229. And: http://bricc.anu.edu.au/ (accessed September 2016).

Kossert, K., Günther, E., 2004. LSC measurements of the half-life of ^{40}K. Appl. Radiat. Isot. 60, 459-464.

Kossert, K. Grau Carles, A., 2008. Study of a Monte Carlo rearrangement model for the activity determination of electron-capture nuclides by means of liquid scintillation counting. Appl. Radiat. Isot. 66, 998-1005.

Kossert, K., Grau Carles, A., 2010. Improved method for the calculation of the counting efficiency of electron-capture nuclides in liquid scintillation samples. Appl. Radiat. Isot. 68, 1482-1488.

Kossert, K., Nähle, O.J., Ott, O., Dersch, R., 2012. Activity determination and nuclear decay data of ^{177}Lu. Appl. Radiat. Isot. 70, 2215-2221.

Kossert, K., Jörg, G., Lierse v. Gostomski, Ch., 2013. Experimental half-life determination of ^{176}Lu. Appl. Radiat. Isot. 81, 140-145.

Kossert, K., Nähle, O.J., 2014. Long-term measurements of ^{36}Cl to investigate potential solar influence on the decay rate. Astropart. Phys. 55, 33-36.

Kossert, K., Cassette, Ph., Grau Carles, A., Jörg, G., Lierse v. Gostomski, Ch., Nähle, O., Wolf, Ch., 2014. Extension of the TDCR model to compute counting efficiencies for radionuclides with complex decay schemes. Appl. Radiat. Isot. 87, 242-248.

Kossert, K., Nähle, O.J., 2015. Disproof of solar influence on the decay rates of ^{90}Sr/^{90}Y. Astropart. Phys. 69, 18-23.

Kossert, K., Broda, R., Cassette, Ph., Ratel, G., Zimmerman, B., 2015. Uncertainty determination for activity measurements by means of the TDCR method and the CIEMAT/NIST efficiency tracing technique. Metrologia 52, S172-S190.

Kossert, K., Mougeot, X., 2015. The importance of the beta spectrum calculation for accurate activity determination of ^{63}Ni by means of liquid scintillation counting. Appl. Radiat. Isot. 101, 40-43.

Kossert, K., Marganiec-Gałązka, J., Mougeot, X., Nähle, O.J., 2018. Activity determination of ^{60}Co and the importance of its beta spectrum. Appl. Radiat. Isot. 134, 212-218.

Kossert, K., Sabot, B., Cassette, P., Coulon, R., Liu, H., 2020. On the photomultiplier-tube asymmetry in TDCR systems. Appl. Radiat. Isot., 163 (2020) 109223.

Kossert, 2021. On the photomultiplier-tube asymmetry in liquid scintillation counters for the CIEMAT/NIST efficiency tracing method. Appl. Radiat. Isot., 170 (2021) 109624.

Kossert, K., Mougeot, X., 2021. Improved activity standardization of ^{90}Sr/^{90}Y by means of liquid scintillation counting. Appl. Radiat. Isot. 168 109478.

Kossert, K., Nähle, O.J., Honig, A., Röttger, S., 2022. Activity standardization by means of liquid scintillation counting and determination of the half-life of ^{89}Zr. Appl. Radiat. Isot. 181, 110078.

Leutz, H., Schulz, G., Wenninger, H., 1965. The decay of potassium-40. Zeitschrift f. Physik 187, 151-164.

Marganiec-Gałązka, J., Nähle, O.J., Kossert, K., 2017. Activity determination of ^{88}Y by means of 4πβ(LS)-γ coincidence counting. J. Radioanal. Nucl. Chem. 314, 599-604.

Merrihue C. and Turner G., 1966. Potassium-argon dating by activation with fast neutrons. J. Geophys. Res. 71, 2852–2857.

Morgan, L. E., Santiago Ramos, D. P., Davidheiser-Kroll, B., Faithfull, J., Lloyd, N.S., Ellam, R.M., Higgins, J.A., 2018. High-precision ^{41}K/^{39}K measurements by MC-ICP-MS indicate terrestrial variability of δ^{41}K. J. Anal. At. Spectrom., 33, 175-186.

Mougeot, X., Bisch, C., 2014. Consistent calculation of the screening and exchange effects in allowed β^- transitions. Phys. Rev. A 90, 012501.

Mougeot, X., 2017. BetaShape: a new code for improved analytical calculations of beta spectra. EPJ Web Conf. 146, 12015.

Mougeot, X., 2018. Improved calculations of electron capture transitions for decay data and radionuclide metrology Appl. Radiat. Isot. 134, 225-232.

Mougeot, X., 2019. Towards high-precision calculation of electron capture decays. Appl. Radiat. Isot. 154, 108884.

Mougeot, X., 2021. BetaShape – v2.2, http://www.lnhb.fr/rd-activities/spectrum-processing-software/, website assessed: 21 July 2021.

Nähle, O., Kossert, K., Cassette, Ph., 2010. Activity standardization of ^{3}H with the new TDCR system at PTB. Appl. Radiat. Isot. 68, 1534-1536.

Nähle, O., Kossert, K., 2011. Comparison of the TDCR method and the CIEMAT/NIST method for the activity determination of beta emitting nuclides. LSC2010, Advances in LS Spectrometry: Proceedings of the 2010 International Conference on LS Spectrometry, Paris, France, 6-10 September 2010, edited by Ph. Cassette, Radiocarbon, The University of Arizona, Tucson, Arizona, USA, ISBN 978-0-9638314-7-7, 313-320.

Nähle, O., Zhao, Q., Wanke, C., Weierganz, M., Kossert, K., 2014. A portable TDCR system. Appl. Radiat. Isot. 87, 249-253.

Naumenko, M.O., Mezger, K., Nägler, T.F., Villa, I.M., 2013. High precision determination of the terrestrial ^{40}K abundance. Geochim. Cosmochim. Acta 122, 353–362.

Naumenko-Dèzes, M.O., Nägler, T.F., Mezger, K., Villa, I.M., 2018. Constraining the ^{40}K decay constant with ^{87}Rb-^{87}Sr – ^{40}K-^{40}Ca chronometer intercomparison. Geochim. Cosmochim. Acta 220, 235–247.

Nucléide – Lara, 2022. Library for gamma and alpha emissions, http://www.nucleide.org/Laraweb/index.php (accessed July 2022).

Renne P. R., Mundil R., Balco G., Min K., Ludwig K. R., 2010. Joint determination of ^{40}K decay constants and ^{40}Ar*/^{40}K for the Fish Canyon sanidine standard, and improved accuracy for ^{40}Ar/^{39}Ar geochronology. Geochim. Cosmochim. Acta 74, 5349–5367.

Renne, P. R., Balco, G., Ludwig, K. R., Mundil, R., Min, K., 2011. Response to the comment by W.H. Schwarz et al. on "Joint determination of ^{40}K decay constants and ^{40}Ar*/^{40}K for the Fish Canyon sanidine standard, and improved accuracy for ^{40}Ar/^{39}Ar geochronology" by P.R. Renne et al. (2010). Geochim. Cosmochim. Acta 75, 5097–5100.

Schaen, A.J, Jicha, B.R., Hodges, K.V., Vermeesch, P., Stelten, M.E., Mercer, C.M., Phillips, D., Rivera, T.A., Jourdan, F., Matchan, E.L., Hemming, S.R., Morgan, L.E., Kelley, S.P., Cassata, W.S., Heizler, M.T., Vasconcelos, P.M., Benowitz, J.A., Koppers, A.P.P., Mark, D.F., Niespolo, E.M., Sprain, C.J., Hames, W.E., Kuiper, K.F., Turrin, B.D., Renne, P.R., Ross, J., Nomade, S., Guillou, H., Webb, L.E., Cohen, B.A., Calvert, A.T., Joyce, N., Ganerød, M., Wijbrans, J., Ishizuka, O., He, H., Ramirez, A.,. Pfänder, J.A., Lopez-Martínez, M., Qiu, H., Singer, B.S., 2020. Interpreting and reporting ^{40}Ar/^{39}Ar geochronologic data. GSA Bulletin 2020; 133 (3-4): 461–487. doi: https://doi.org/10.1130/B35560.1.

Schwarz, W. H., Kossert, K., Trieloff, M. and Hopp, J., 2011. Comment on the "Joint determination of ^{40}K decay constants and ^{40}Ar*/^{40}K for the fish canyon sanidine standard, and improved

accuracy for $^{40}Ar/^{39}Ar$ geochronology" by Paul R. Renne et al. Geochim. Cosmochim. Acta 75, 5094–5096.

Schötzig, U., Schrader, H., 2000. Halbwertszeiten und Photonen-Emissionswahrscheinlichkeiten von häufig verwendeten Radionukliden. PTB-report PTB-Ra-16 5th Edition, Braunschweig, Germany.

Sima, O., Arnold, D., Dovlete, C., 2001. GESPECOR – a versatile tool in gamma-rayspectrometry. J. Radioanal. Nucl. Chem. 248, 359–364.

Suttle, A. D. Jr, Libby, W. F., 1955. Absolute assay of beta radioactivity in thick solids – Application to naturally radioactive potassium. Anal. Chem. 22, 921-927.

Teflon™ FEP, Information Bulletin, 2017. The Chemours Company. https://www.teflon.com/en/-/media/files/teflon/teflon-fep-film-tech-bulletin.pdf (accessed May 2022).

Thiam, C., Bobin, C., Bouchard, J., 2010. Simulation of Cherenkov photons emitted in photomultiplier windows induced by Compton diffusion using the Monte Carlo code GEANT4. Appl. Radiat. Isot. 68, 1515-1518.

Tilley, D. R., Madansky, L., 1959. Search for positron emission in ^{40}K Phys. Rev. 116, 413-415.

Towner, I.S., Hardy, J.C., 2008. Improved calculation of the isospin-symmetry-breaking corrections to superallowed Fermi β decay. Phys. Rev. C 77, 025501.

Wang, K., Jacobsen, S.B., 2016. An estimate of the bulk silicate earth potassium isotopic composition based on MC-ICPMS measurements of basalts. Geochim. Cosmochim. Acta 178, 223–232.

Wang, M., Huang, W.J., Kondev, F.G., Audi, G., 2021. The AME2020 atomic mass evaluation (II). Tables, graphs and references. Chin. Phys. C 45, 030003.

Wielandt, D., Bizzarro, M., 2011. A TIMS-based method for the high precision measurements of the three-isotope potassium composition of small samples. J. Anal. At. Spectrom. 26, 366–377.

Table 1

The relevant information on the EC transitions needed for the MICELLE calculations were derived from results obtained by means of the BetaShape code (Mougeot, 2018, 2019, 2021).

	EC transition (see Figure 1)	
	$EC_{0,1}$	**$EC_{0,0}$**
Nature of the transition	1st forbidden unique	3rd forbidden unique
P_K	0.7548(7)	0.8908(7)
P_{L1}	0.1044(6)	0.0956(5)
P_{L2}	$2.401(17)\cdot10^{-4}$	$2.202(16)\cdot10^{-4}$
P_{L3}	0.1167(9)	$6.214(31)\cdot10^{-4}$
$P_{M+}=1-P_K-P_{L1}-P_{L2}-P_{L3}$	0.0239(13)	0.0128(9)

Table 2

Overview on gamma-ray spectrometry measurements with the K40-Bern solution as measured and analyzed 2005. For this analysis, the emission probability of the 1461 keV gamma-rays was assumed to be 0.1067(13) as stated by Schötzig and Schrader (2000).

Sample identifier	**Total counting time**	**Activity concentration***
Background	143 h	-
2004-1846	138 h	39.02(65) Bq/g
2004-1847	42.4 h	39.44(66) Bq/g

* The activity concentrations were determined assuming $P_\gamma = 0.1067$. Multiply by 1.03693 to obtain activity concentrations with the gamma emission probability from this work ($P_\gamma = 0.1029$).

Table 3

Uncertainty budget for the activity concentration of the K40-Bern solution when using low-level gamma-ray spectrometry. All uncertainties are stated as standard uncertainties (k=1).

Uncertainty component	**Relative uncertainty**
Mass of solution	0.025%
Net peak area	0.2%
Gamma-ray emission probability (here, P_γ = 0.1067(13) was assumed)	1.22%
Detection efficiency at 1461 keV	1.102%
Background	0.01%
Correction for self-absorption	0.01%
Correction for slight geometry variations	0.01%
Combined	**1.656%**
Combined without $u(P_\gamma)$	**1.12%**

Table 4

Uncertainty budget for the activity concentration of the K40-Bern solution determined by the CNET method. All uncertainties are stated as standard uncertainties (k=1).

Component	**Relative uncer-tainty**
Standard deviation of result obtained from 4 LS samples	0.125%
Weighing for LS samples	0.016%
Dead time	0.1%
Background	0.05%
Adsorption	0.03%
^{3}H activity	0.016%
Impurity correction (^{137}Cs, detected)	0.008%
Ionization quenching	0.02%
Photon backscattering	0.033%
P_{β^-}, $P_{\mathrm{EC}_{0,1}}$, and $P_{\mathrm{EC}_{0,0}}$	0.164%
Model and other decay data	0.1%
PMT asymmetry	0.01%
Decay correction	0.001%
Combined uncertainty	**0.261%**
Combined uncertainty without uncertainty component assigned to P_{β^-}, $P_{\mathrm{EC}_{0,1}}$ and $P_{\mathrm{EC}_{0,0}}$	**0.203%**

Table 5

Overview of the maximum net counting rates, background counting rates and counting efficiencies for various experimental configurations. For the TDCR measurements, the stated counting efficiency is related to the logical sum of double coincidences.

Experiment / solution	**LS counter**	**Type of LS vial**	**Maximum ^{40}K net counting rate R_{net} in s^{-1}**	**Background counting rate R_{bg} in s^{-1}**	**R_{net}/R_{bg}**	**^{40}K counting efficiency**
Kossert and Günther (2004), natural isotopic composition	Wallac 1414	Glass	10.0	0.8	12.0	89.7%
This work, "K40-Bern"	Wallac 1414	Glass	36.8	0.8	47.2	90.3%
This work, "K40-GSC"	Wallac 1414	Glass	147.4	1.2	122.8	90.3%
This work, "K40-GSC"	TriCarb 2800 TR	Glass	148.2	0.8	178.6	90.8%
This work, "K40-GSC"	TDCR-M27	Glass	150.7	4.9	30.8	92.3%
This work, "K40-GSC"	TDCR-M27	PE	147.6	4.7	31.4	92.4%
This work, "K40-GSC"	TDCR-M29	Glass	150.0	3.0	50.0	91.9%
This work, "K40-GSC"	TDCR-M29	PE	146.9	2.9	50.7	92.0%

Table 6

Results for P_{β^-} from the LS spectrum analysis. Experimental LS spectra of various pure beta emitting radionuclides were used to evaluate the contribution of beta decay at low energies.

Reference	**Radionuclide used to estimate shape of beta spectrum at low energies**	P_{β^-}
	^{14}C	0.8948
	^{89}Sr	0.8949
	^{90}Y	0.8954
	^{90}Sr	0.8963
Final result of this work (mean of values given above)		**0.8954(14)**
Bé et al. (2010), DDEP evaluation		0.8925(17)
Chen (2017), NDS evaluation		0.8928(13)
Renne et al. (2011)*		0.8959(4)

* Calculated from their partial decay constants $\lambda_\varepsilon = (5.757 \pm 0.016)\cdot 10^{-11}$ a^{-1} and $\lambda_\beta = (4.9548 \pm 0.0134)\cdot 10^{-10}$ a^{-1}

Table 7

Results of the three individual measurements of the K40-GSC solution by means of gamma-ray spectrometry.

Run No.	Detector	Measurement time in h	$A(^{40}K)$ in Bq*	^{137}Cs decision limit in Bq	^{137}Cs detection limit in Bq
1	#6	133.5	318.5	$4.9 \cdot 10^{-2}$	$7.7 \cdot 10^{-2}$
2	#6	143.0	316.6	$4.0 \cdot 10^{-2}$	$6.3 \cdot 10^{-2}$
3	#9	134.5	315.3	$6.2 \cdot 10^{-2}$	$9.7 \cdot 10^{-2}$
		Unweighted mean:	316.8		

* The activities were determined assuming $P_\gamma = 0.1055$. Multiply by 1.02527 to obtain activities with the gamma emission probability from this work ($P_\gamma = 0.1029$).

Table 8

Uncertainty budget for the activity concentration of the K40-GSC solution when using low-level gamma-ray spectrometry (Example for run #2 with detector #6). All uncertainties are stated as standard uncertainties (k=1).

Uncertainty component	**Relative uncertainty**
Mass of solution	0.02%
Net peak area	0.3%
Gamma-ray emission probability (here, P_γ = 0.1055(11) was assumed)	1.05%
Detection efficiency at 1461 keV[#]	0.8%
Background	0.03%
Correction for self-absorption	0.001%
Correction for slight geometry variations	0.01%
Combined	**1.36%**
Combined without $u(P_\gamma)$	**0.86%**

The following gamma-ray emission probabilities were assumed for the efficiency calibration (Nucléide – Lara, 2022): $P_\gamma(^{60}\text{Co}, 1173.23\ \text{keV}) = 0.9985(3)$; $P_\gamma(^{60}\text{Co}, 1332.49\ \text{keV}) = 0.999826(6)$; $P_\gamma(^{88}\text{Y}, 898.04\ \text{keV}) = 0.937(3)$; $P_\gamma(^{88}\text{Y}, 1836.07\ \text{keV}) = 0.99346(25)$ and $P_\gamma(^{137}\text{Cs}, 661.66\ \text{keV}) = 0.8499(20)$

Table 9

Uncertainty budgets for the activity concentration of the K40-GSC solution measured by two LS counting methods.

Component	**Relative uncertainty**	
	CIEMAT/ NIST	TDCR
Standard deviation of the results shown in Figure 12	0.064%	0.072%
Weighing (LS samples)	0.01%	0.01%
Dead time	0.1%	0.05%
Background	0.03%	0.04%
Adsorption	0.03%	0.03%
TDCR value		0.03%
^{3}H activity	0.016%	
Impurity correction (^{137}Cs, detected)	0.017%	0.017%
Ionization quenching	0.02%	0.02%
Photon backscattering	0.033%	0.033%
$P(\beta^-)$, $P(EC_{0,1})$, and $P(EC_{0,0})$	0.149%	0.15%
Model and other decay data	0.1%	0.1%
PMT asymmetry	0.01%	0.01%
Decay correction	0.001%	0.001%
Combined uncertainty	**0.224%**	**0.214%**
Combined uncertainty without uncertainty component assigned to $P(\beta^-)$,$P(EC_{0,1})$ and $P(EC_{0,0})$	**0.167%**	**0.152%**

Table 10

Results obtained by Kossert and Günther (2004) when determining the ^{40}K half-life by means of LS measurements using salts with natural isotopic composition. The ^{40}K LS counting efficiencies and individual half-life values were recalculated using the same model and input data as in this work. In particular, the decay scheme parameters as determined in this work were used and a correction was applied to allow for the photon backscattering effect.

Sample number	**LS cocktail and salt**	**$\varepsilon(^{3}H)$ in %**	**$\varepsilon(^{40}K)$ in % (original work)**	**$T_{1/2}$ in 10^9 a (original work)**	**Relative statistical uncertainty in %**	**$\varepsilon(^{40}K)$ in % (recalculated)**	**$T_{1/2}$ in 10^9 a (recalculated)**
1	Hionic Fluor, KNO_3	24.040	89.734	1.2491	0.074	90.127	1.2546
5	Hionic Fluor, KNO_3	35.476	90.211	1.2486	0.070	90.592	1.2539
9	Ultima Gold LLT, KNO_3	36.530	90.262	1.2484	0.075	90.641	1.2536
13	Ultima Gold LLT, KNO_3	24.949	89.770	1.2479	0.034	90.161	1.2533
3	Ultima Gold AB, KCl	28.941	89.926	1.2461	0.078	90.314	1.2515
7	Ultima Gold AB, KCl	37.862	90.313	1.2410	0.147	90.704	1.2464
11	Hionic Fluor, KCl	38.826	90.360	1.2553	0.178	90.751	1.2607
15	Hionic Fluor, KCl	29.280	89.939	1.2478	0.086	90.327	1.2532

Table 11

The total ^{40}K half-life determined in this work compared to other selected references.

Reference	$T_{1/2}$ **in** 10^9 **a**	**Relative deviation to the result from this work**
This work	1.2536(27)	-
Bé et al. (2010), DDEP evaluation	1.2504(30)	-0.26%
Chen (2017), NDS evaluation	1.248(3)	-0.45%
Renne et al. (2011)	1.2533(31)	-0.02%
Naumenko-Dèzes et al. (2018)	$1.2607 < T_{1/2} < 1.2639$	0.57% - 0.82%
Suttle and Libby (1955), recalculated*	1.23(4)	-1.88%
Leutz et al. (1965), recalculated**	1.253(10)	-0.05%
Grau Malonda and Grau Carles (2002), reanalyzed	1.249(4)	-0.37%
Kossert and Günther (2004), reanalyzed	1.253(3)	-0.05%
New data evaluation from this work	1.2521(27)	-0.12%

* The original value (1.25(4) 10^9 a) was recalculated with a newer result for the ^{40}K abundance in natural K and adjustment of original data.

** The original value and its uncertainty (1.266(7) 10^9 a) were recalculated with a newer result for the ^{40}K abundance in natural K and adjustment of original data.

Table 12

The total and partial ^{40}K decay constants determined in this work compared to the revised values of Renne et al. (2011).

Reference	λ_{total} **in** a^{-1}	$u(\lambda_{total})/\lambda_{total}$	λ_{β} **in** a^{-1}	$u(\lambda_{\beta})/\lambda_{\beta}$	λ_{EC} **in** a^{-1}	$u(\lambda_{EC})/\lambda_{EC}$
Experimental result of this work	$5.5294 \cdot 10^{-10}$	0.214%	$4.9510 \cdot 10^{-10}$	0.265%	$5.7837 \cdot 10^{-11}$	1.355%
Renne et al. (2011)	$5.5305 \cdot 10^{-10}$	0.244%	$4.9548 \cdot 10^{-10}$	0.270%	$5.757 \cdot 10^{-11}$	0.280%
Relative deviation:	0.02%		0.08%		-0.46%	
New data evaluation from this work	$5.536 \cdot 10^{-10}$	0.217%	$4.954 \cdot 10^{-10}$	0.222%	$5.822 \cdot 10^{-11}$	0.223%

Figures with captions

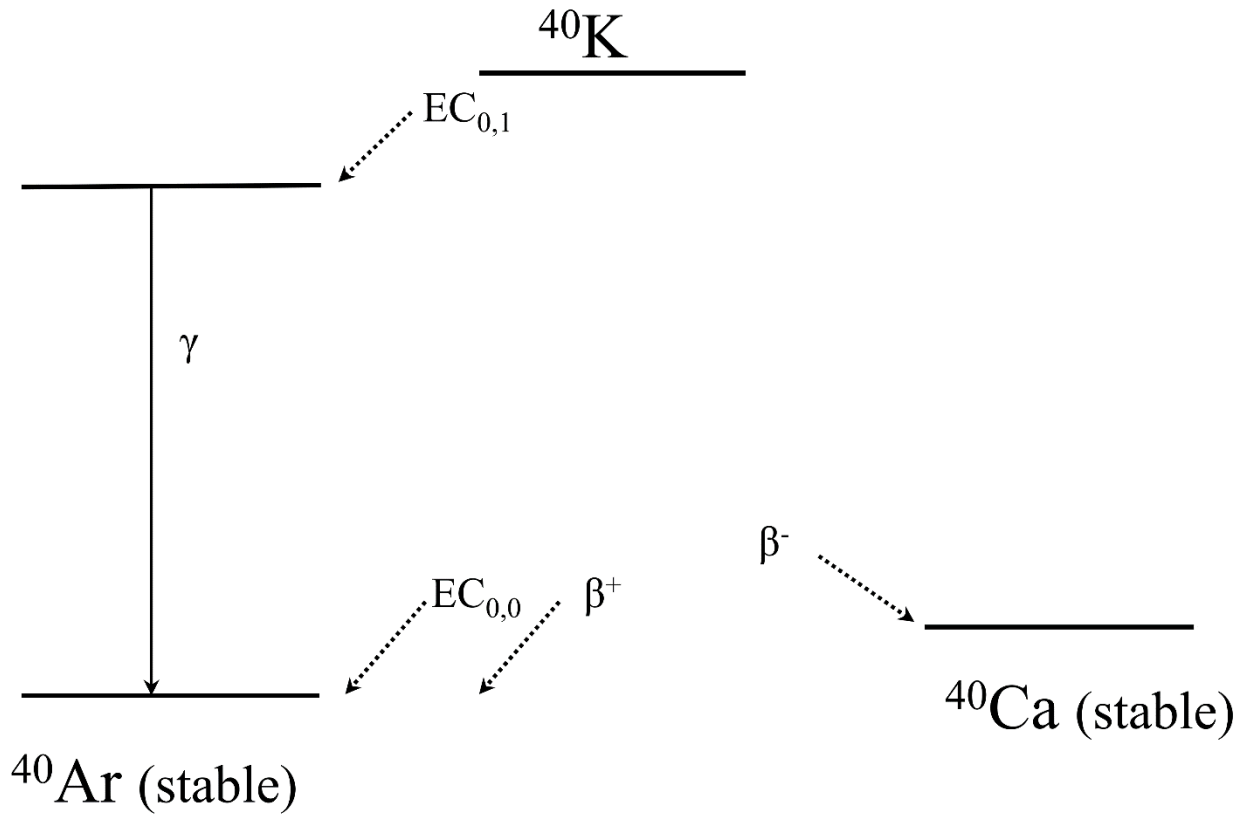

Figure 1

Decay scheme of ^{40}K. The dominant transition is the beta minus transition.

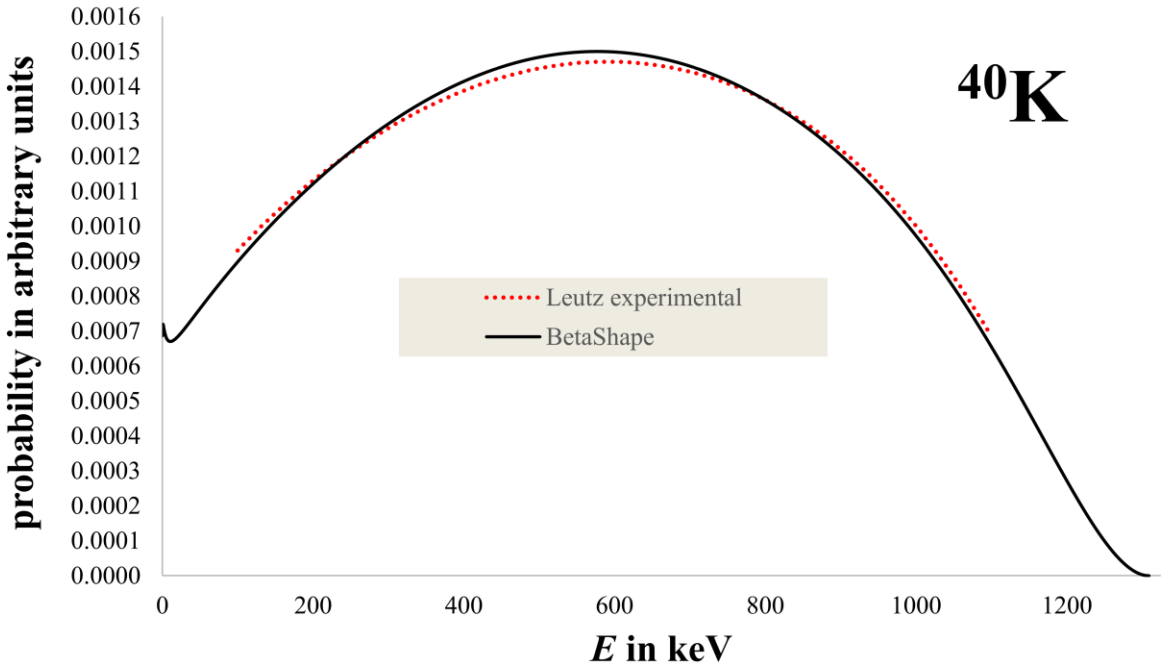

Figure 2

Spectrum of the 3rd forbidden unique beta transition computed with BetaShape taking screening corrections and the atomic exchange effect into account. The dotted spectrum was calculated with a shape-factor derived from experimental data of Leutz et al. (1965) who measured the beta spectrum in the energy range from 100 keV to 1100 keV.

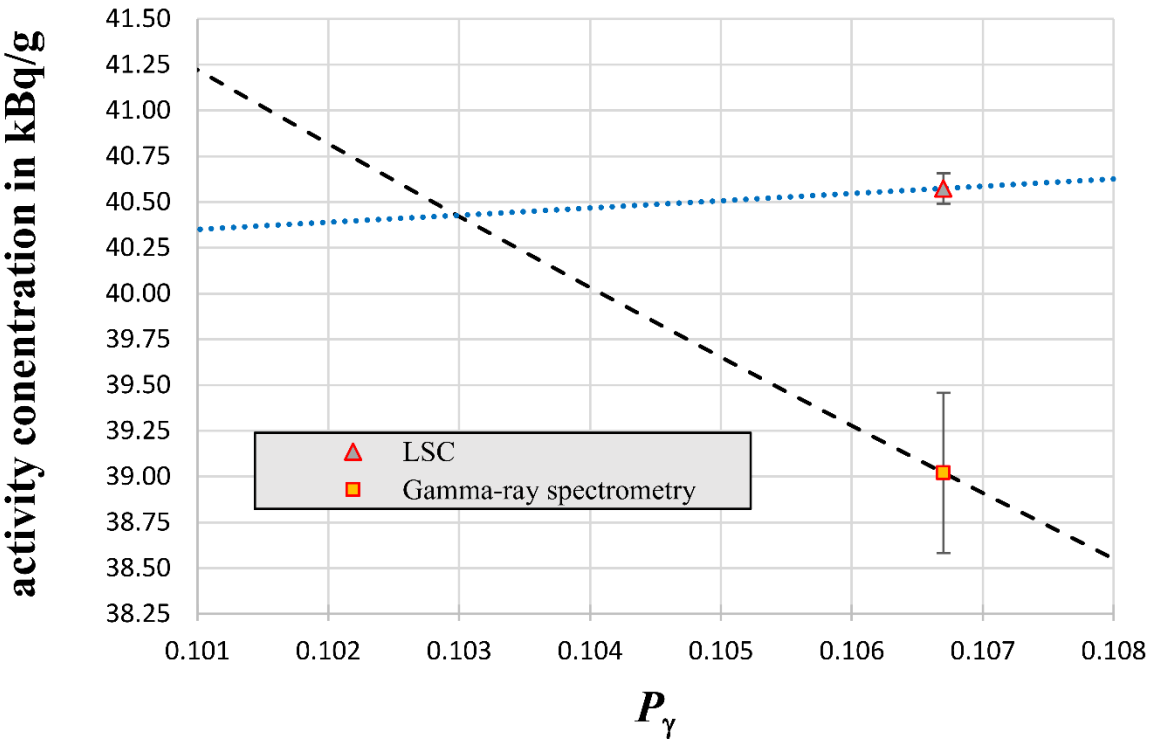

Figure 3

Activity concentration of the K40-Bern solution from LS counting and gamma-ray spectrometry as a function of the gamma emission probability P_γ. The uncertainty bars of the measured values at P_γ=0.1067 represent the total combined standard uncertainty without an uncertainty assigned to P_γ.

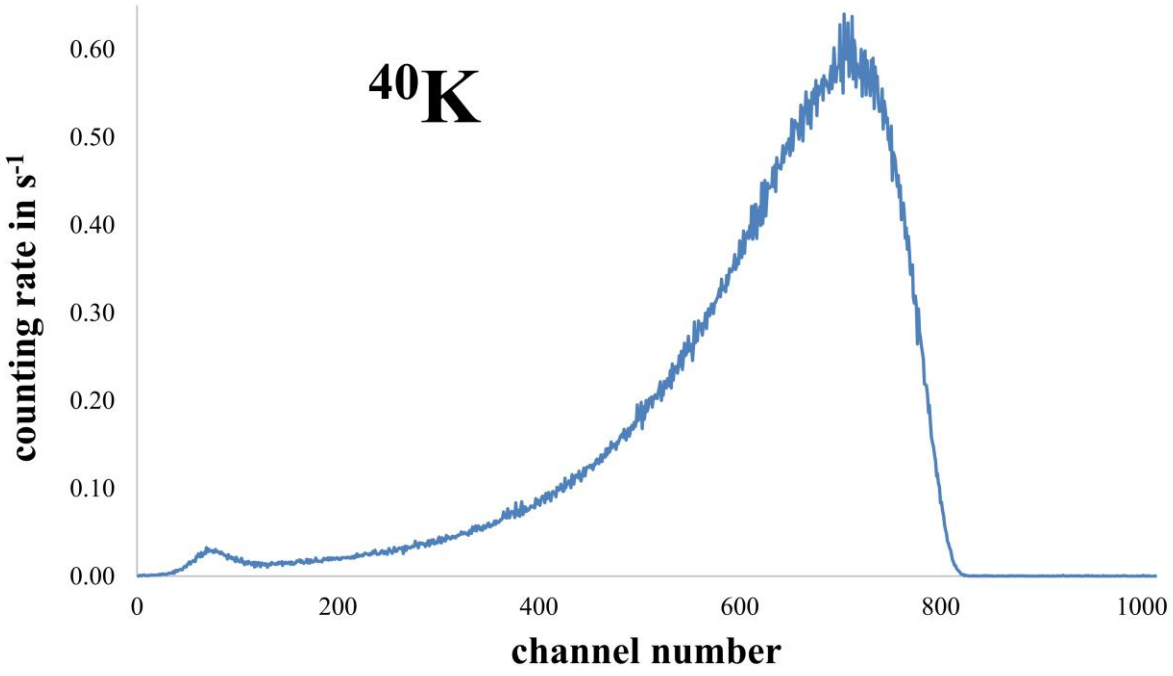

Figure 4

Measured spectrum of an LS sample with the solution K40-GSC in a glass vial. The measurement was carried out in a Wallac 1414 counter with logarithmic amplification. A background spectrum has been subtracted.

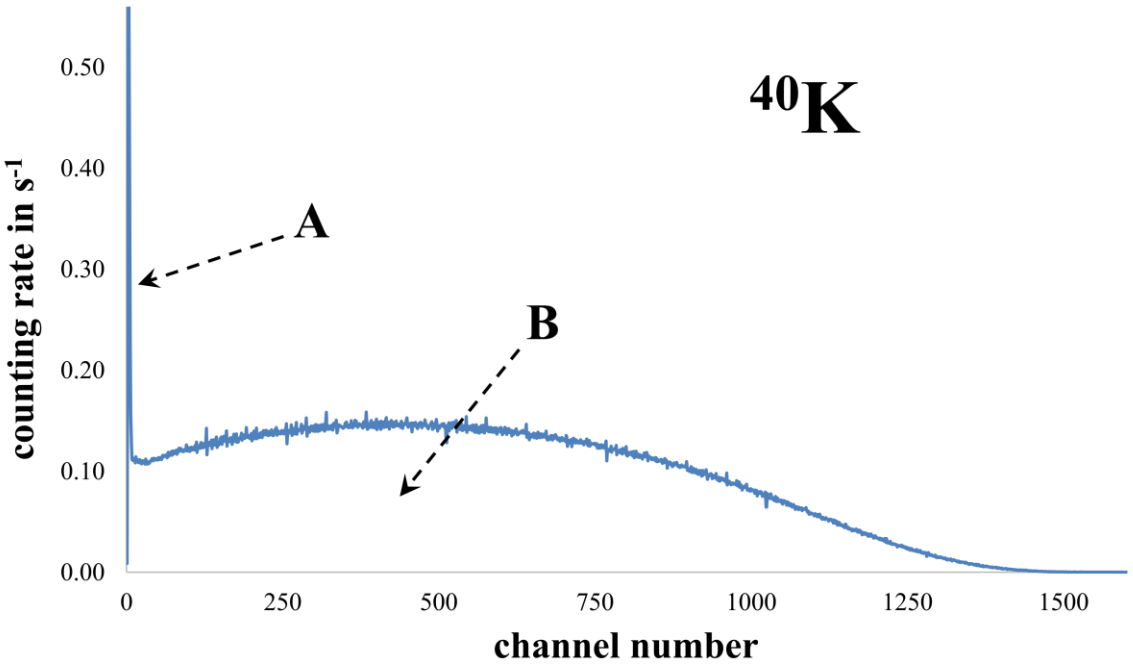

Figure 5

Net spectrum of an LS source with the solution K40-GSC in a glass vial measured in a TriCarb 2800 TR counter. The overall counting time was 16 h and the net spectrum corresponds to about $8.32 \cdot 10^6$ counts. The peak at low channel numbers ("A") results from detection of EC decays while the wide area "B" is mainly due to detection of beta decay events.

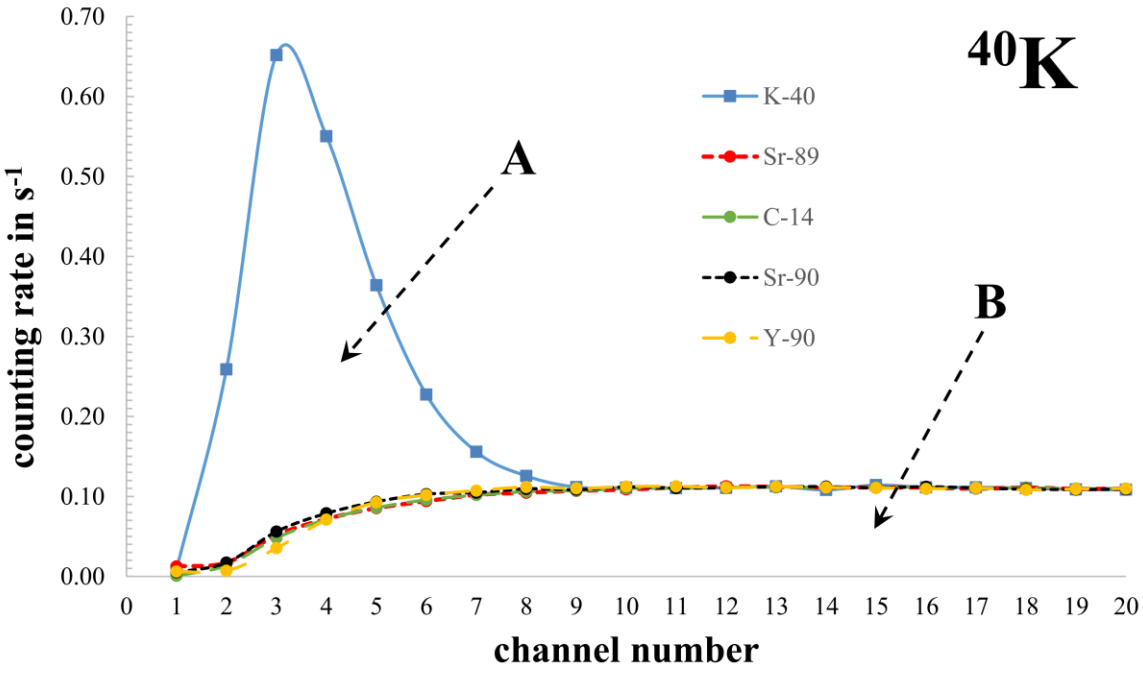

Figure 6

Net spectrum of a ^{40}K LS source measured in a TriCarb 2800 TR counter (as in Figure 5) at low channel numbers. The net LS spectra of other beta emitters were adjusted in the range from channel 10 to channel 20 to evaluate the contributions to the areas A and B of the ^{40}K spectrum at channel numbers below 10.

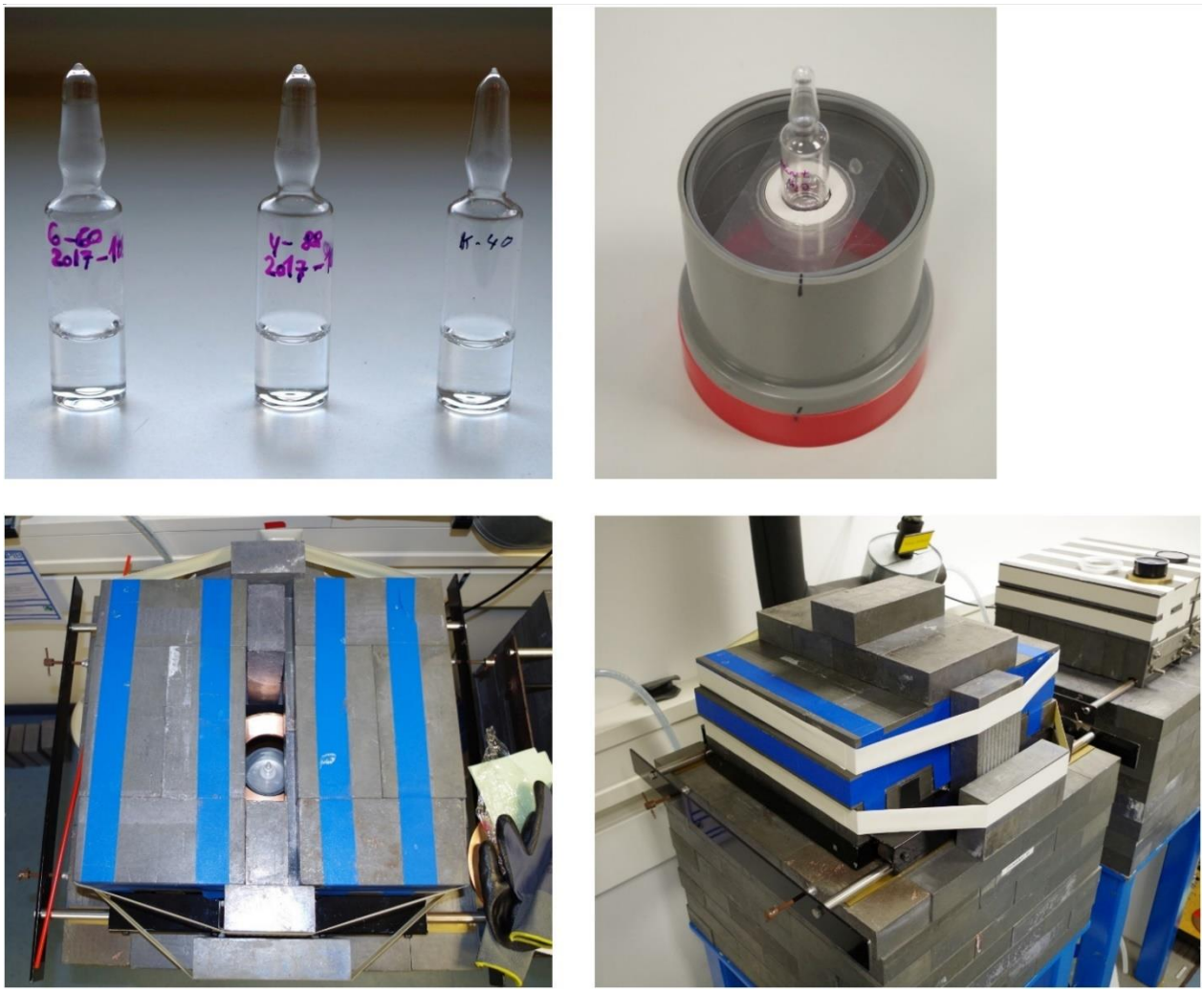

Figure 7

Flame-sealed PTB glass ampoules with standard solutions of ^{60}Co, ^{88}Y and the K40-GSC solution (top left); a custum-built sample holder with a background sample (top right); sample with holder in measurement position (bottom left); and counter with complete Pb shielding when sample is in position (bottom right).

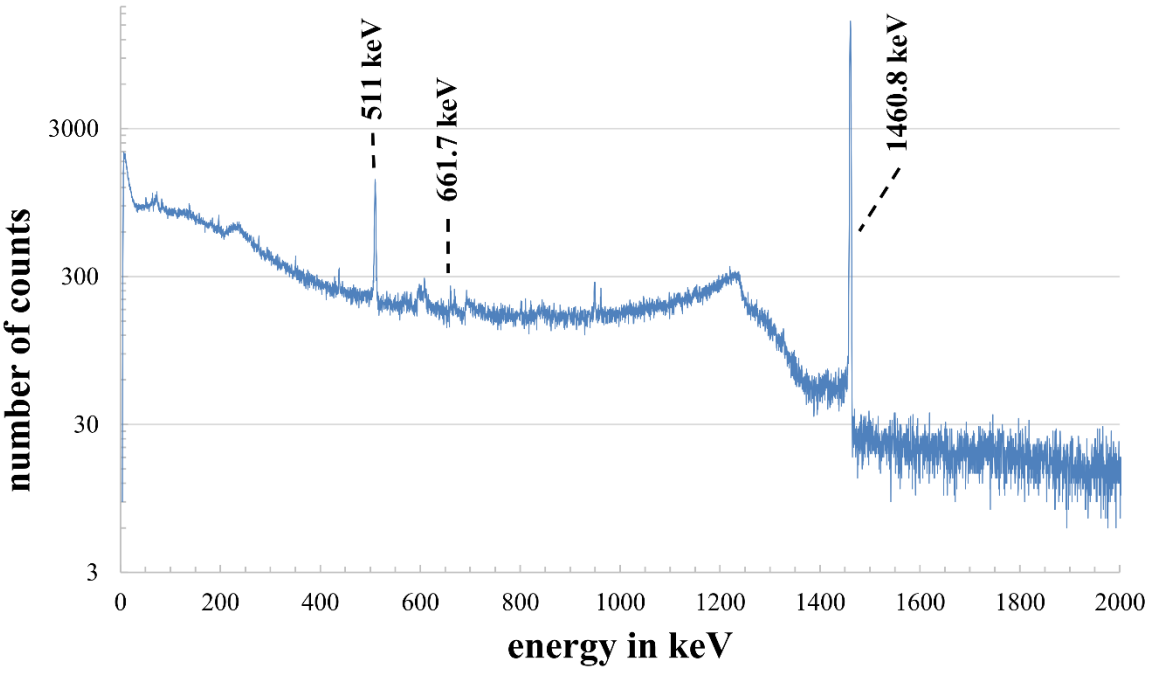

Figure 8

Gamma-ray spectrum of the K40-GSC solution measured with the HPGe detector #6 (Run #2). The duration of this measuement was 143 h.

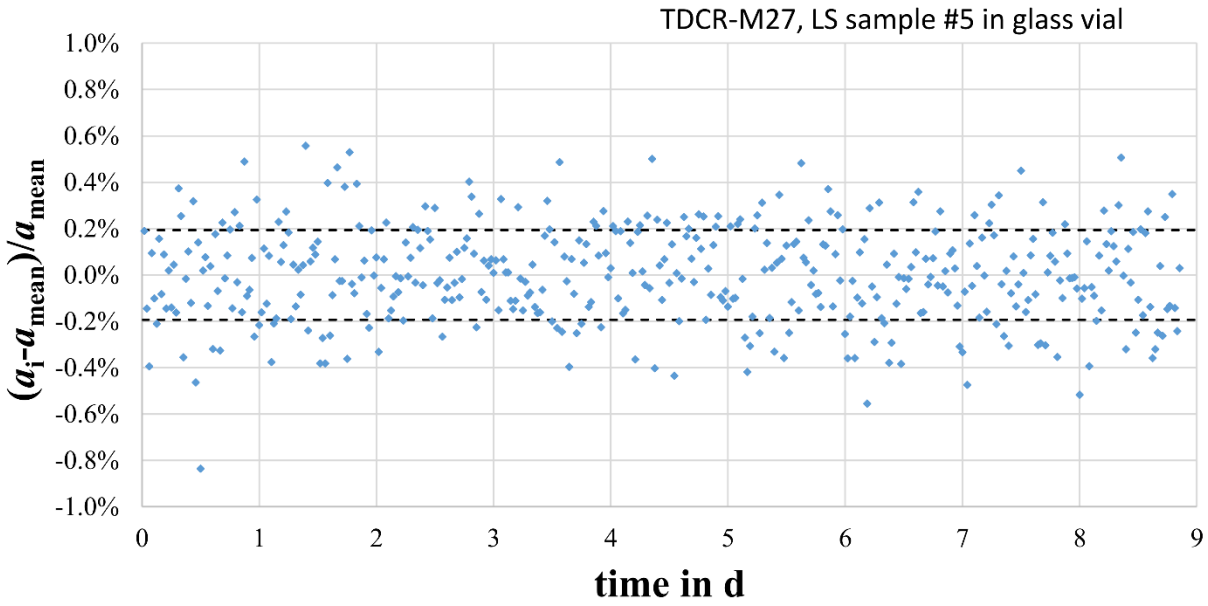

Figure 9

Residuals $(a_i-a_{mean})/a_{mean}$ for LS sample #5 measured for about 9 days in the counter TDCR-M27. About 65% of the data are within the band represented by the dashed lines. This range (±0.193%) is defined by the Poisson uncertainty for a single measurement with a duration of 1800 s.

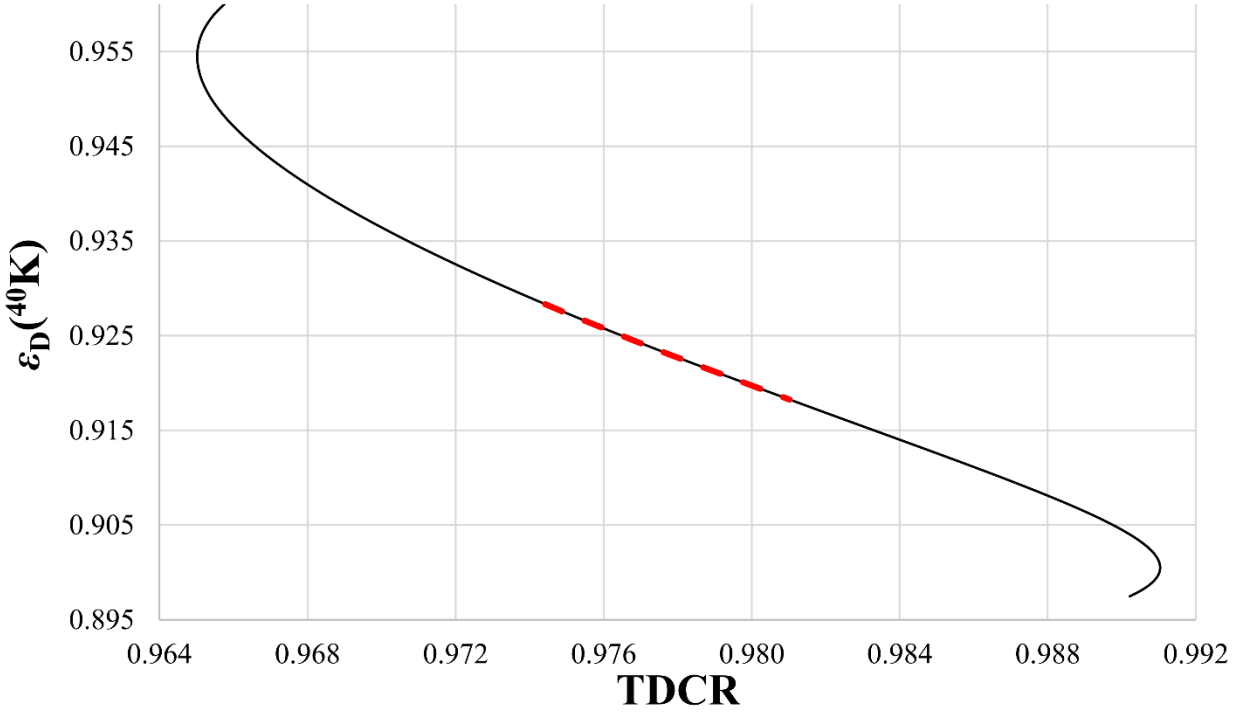

Figure 10

Computed ^{40}K double counting efficiency ε_D as a function of the TDCR parameter. The ambiguity is a well-known effect which occurs for several radionuclides with complex decay schemes (see, e.g., Broda et al. 2007). The experimental data from this work define the region of interest which is represented by the red dashed line in the figure.

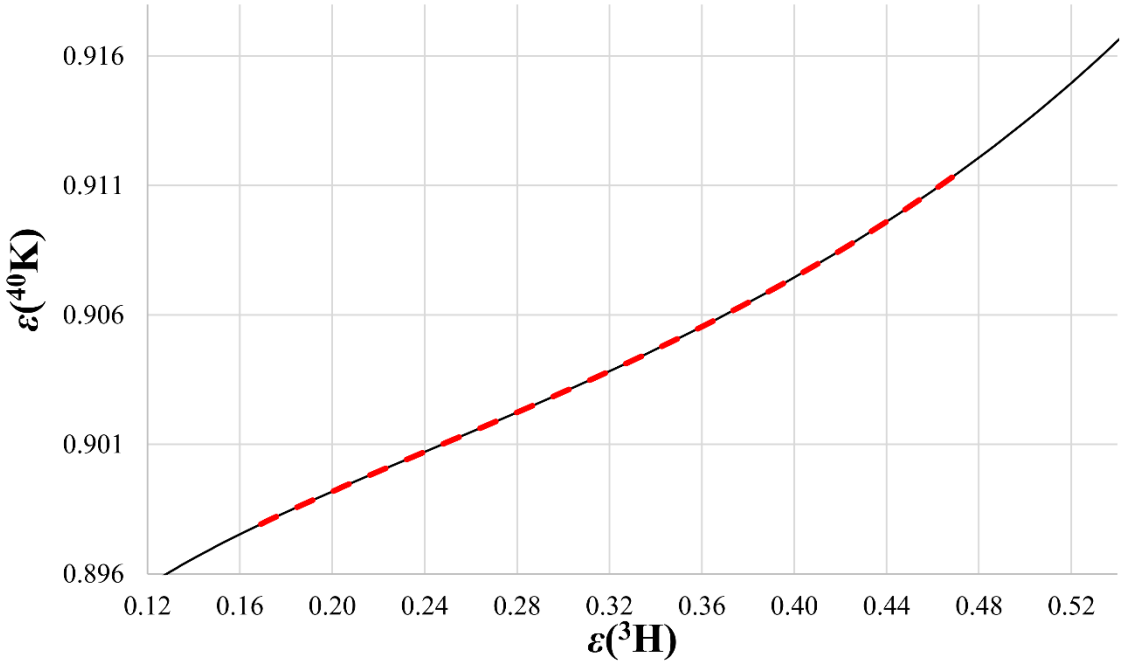

Figure 11

Computed ^{40}K counting efficiency as a function of the ^{3}H counting efficiency to apply the CNET method. The experimental data from this work define the the region of interest which is represented by the red dashed line in the figure.

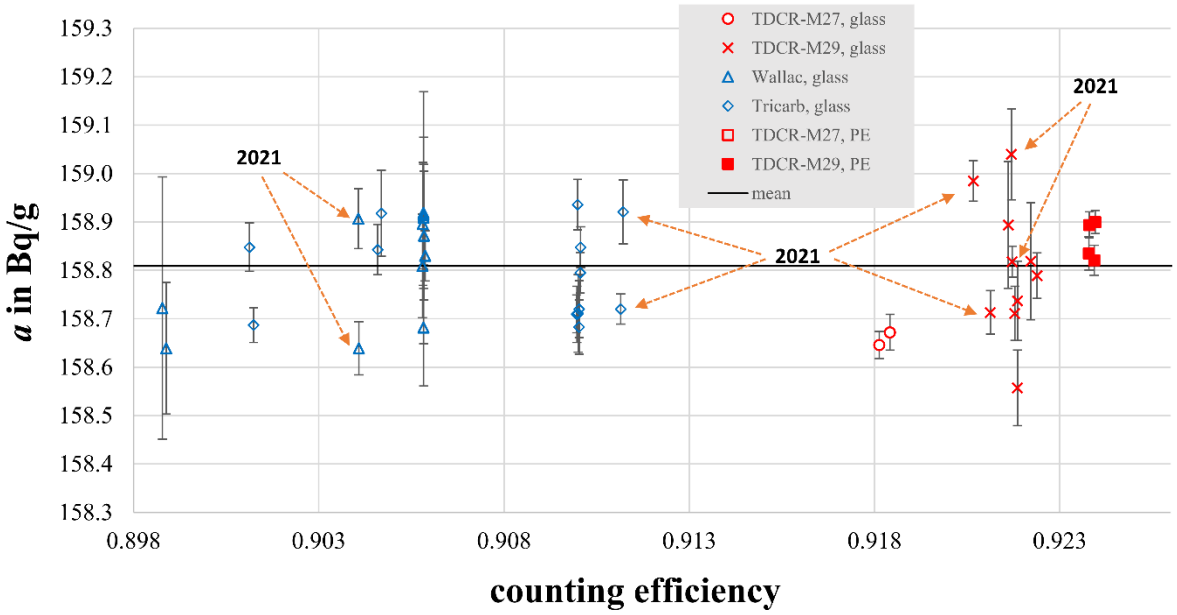

Figure 12

Activity concentration of the K40-GSC solution as obtained for the CNET method and the TDCR method. The uncertainty bars represent only a statistical component calculated as a standard deviation of the mean of several repeat measurements.

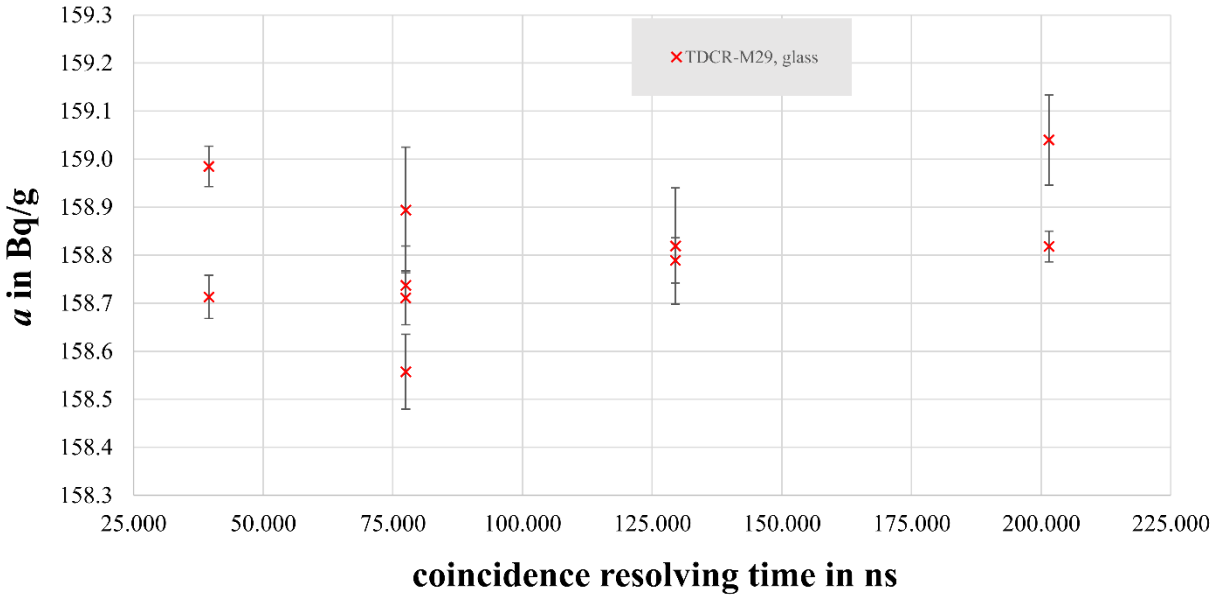

Figure 13

Activity concentration as obtained from the measurements of glass vials in TDCR-M29 as a function of the coincidence resolving time. The uncertainty bars represent only a statistical component calculated as a standard deviation of the mean of several repeat measurements. The same data are also incldued in Figure 12.